Constant Growth Rate Can Be Supported by Decreasing Energy Flux and Increasing Aerobic Glycolysis

Citation: Slavov, Nikolai, Bogdan A. Budnik, David Schwab, Edoardo M. Airoldi, and Alexander van Oudenaarden. "Constant Growth Rate Can Be Supported by Decreasing Energy Flux and Increasing Aerobic Glycolysis." Cell Reports 7, no. 3 (May 2014): 705–714.

As Published: http://dx.doi.org/10.1016/j.celrep.2014.03.057

Publisher: Elsevier

Persistent URL: http://hdl.handle.net/1721.1/96921

Version: Final published version: final published article, as it appeared in a journal, conference proceedings, or other formally published context

Cell Reports
Report

Constant Growth Rate Can Be Supported by Decreasing Energy Flux and Increasing Aerobic Glycolysis

Nikolai Slavov,[1,2,3,4,*] Bogdan A. Budnik,[2] David Schwab,[5] Edoardo M. Airoldi,[2,3] and Alexander van Oudenaarden[1,4,*]
[1]Departments of Physics and Biology and Koch Institute for Integrative Cancer Research, Massachusetts Institute of Technology, Cambridge, MA 02139, USA
[2]Department of Statistics and FAS Center for Systems Biology, Harvard University, Cambridge, MA 02138, USA
[3]Broad Institute of MIT and Harvard, Cambridge, MA 02142, USA
[4]Hubrecht Institute, Royal Netherlands Academy of Arts and Sciences and University Medical Center Utrecht, Uppsalalaan 8, 3584 CT Utrecht, the Netherlands
[5]Department of Physics and Lewis-Sigler Institute, Princeton University, Princeton, NJ 08544, USA
*Correspondence: nslavov@alum.mit.edu (N.S.), a.vanoudenaarden@hubrecht.eu (A.v.O.)
http://dx.doi.org/10.1016/j.celrep.2014.03.057

SUMMARY

Fermenting glucose in the presence of enough oxygen to support respiration, known as aerobic glycolysis, is believed to maximize growth rate. We observed increasing aerobic glycolysis during exponential growth, suggesting additional physiological roles for aerobic glycolysis. We investigated such roles in yeast batch cultures by quantifying O_2 consumption, CO_2 production, amino acids, mRNAs, proteins, posttranslational modifications, and stress sensitivity in the course of nine doublings at constant rate. During this course, the cells support a constant biomass-production rate with decreasing rates of respiration and ATP production but also decrease their stress resistance. As the respiration rate decreases, so do the levels of enzymes catalyzing rate-determining reactions of the tricarboxylic-acid cycle (providing NADH for respiration) and of mitochondrial folate-mediated NADPH production (required for oxidative defense). The findings demonstrate that exponential growth can represent not a single metabolic/physiological state but a continuum of changing states and that aerobic glycolysis can reduce the energy demands associated with respiratory metabolism and stress survival.

INTRODUCTION

Understanding cell growth is essential to both basic science and treating diseases associated with deregulated cell growth, such as cancer. Accordingly, cell growth has been studied extensively, from the pioneering work of Krebs and Eggleston (1940) and Monod (1949) to recent discoveries (DeBerardinis et al., 2007; Slavov et al., 2011; Scott et al., 2010; Youk and van Oudenaarden, 2009; Clasquin et al., 2011; Chang et al., 2013). Although the major biochemical networks were identified by the 1950s (Krebs and Eggleston, 1940; Monod, 1949), understanding the coordination between these pathways in time remains a major challenge and opportunity to systems biology (Hartwell et al., 1999; McKnight, 2010; Slavov and Botstein, 2011). The challenge stems from the fact that both cell growth and metabolism may take alternative parallel paths. For example, cells can produce energy either by fermenting glucose to lactate/ethanol to generate two ATP molecules per glucose molecule or by respiration (oxidative phosphorylation) to generate substantially more (between 16 and 36 depending on the estimate) ATP molecules per glucose molecule. The estimates for the in vivo efficiency of oxidative phosphorylation vary widely depending on the measurement method and the underlying assumptions. These estimates come from (1) measuring ATP production during fermentative growth and assuming it equals the ATP production and demand during respiratory growth (von Meyenburg, 1969; Verduyn et al., 1991; Famili et al., 2003), (2) in vivo ^{31}P NMR flux measurements (Campbell et al., 1985; Gyulai et al., 1985; Portman, 1994; Sheldon et al., 1996), and (3) in vitro measurements with isolated mitochondria (Rich, 2003).

Although respiration has higher ATP yield per glucose, cancer/yeast cells tend to ferment most glucose into lactate/ethanol even in the presence of sufficient oxygen to support respiration, a phenomenon known as aerobic glycolysis. This apparently counterintuitive metabolic strategy of using the less efficient pathway is conserved from yeast to human and has been recognized as a hallmark of cancer (Vander Heiden et al., 2009; Hanahan and Weinberg, 2011). Numerous competing models have been proposed to explain aerobic glycolysis both in yeast and in human (Warburg, 1956; Newsholme et al., 1985; De Deken, 1966; Pfeiffer et al., 2001; Gatenby and Gillies, 2004; Molenaar et al., 2009; Vander Heiden et al., 2009; Vazquez et al., 2010; Shlomi et al., 2011; Lunt and Vander Heiden, 2011; Ward and Thompson, 2012).

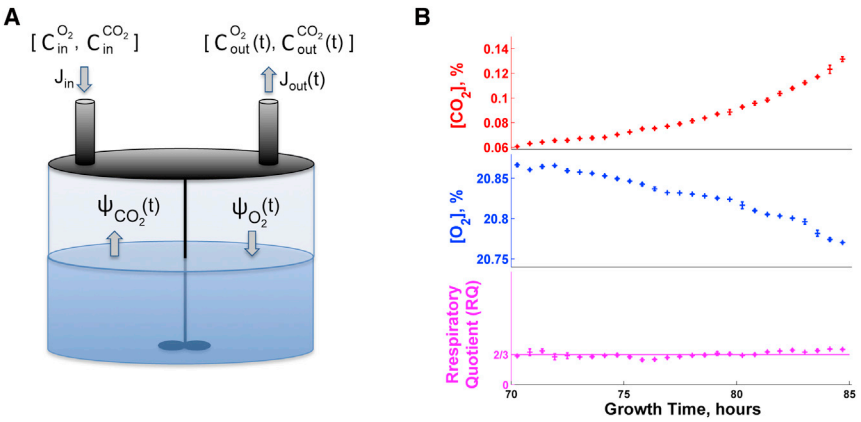

Figure 1. Experimental Design for Precision Measurements of O_2 Uptake and CO_2 Production in Time

(A) A conceptual schematic of the method used for precision measurements of O_2 and CO_2 fluxes in low-density yeast cultures; C_{in} are the concentrations of gases in the air entering the reactor at rate J_{in}, and the C_{out} are the concentrations of gases existing the reactor at rate J_{out}.

(B) The respiratory quotient (RQ) estimated from O_2 and CO_2 concentrations measured in a low-density yeast culture growing on ethanol as a sole source of carbon and energy equals the RQ estimate from mass conservation (2/3); the culture was inoculated at a density of 1,000 cells/ml, and measurements began 70 hr after inoculation, when the culture had reached a density of about 10^5 cells/ml.

Error bars denote SDs. See Figure S1 and the Supplemental Information for more control experiments and details.

Although the models propose different and often conflicting mechanisms, they aim to explain aerobic glycolysis as a metabolic strategy for maximizing the cellular growth rate. However, in some cases slowly growing or even quiescent cells exhibit aerobic glycolysis (Boer et al., 2008; Lemons et al., 2010; Slavov and Botstein, 2013). Theoretical models of aerobic glycolysis are limited by the many incompletely characterized tradeoffs of respiration and fermentation, such as the effects of aerobic glycolysis on signaling mechanisms (Chang et al., 2013). Further limitations stem from missing estimates for key metabolic fluxes. For example, depending on whether the increase in the flux of fermented glucose compensates for the low efficiency of fermentation, aerobic glycolysis may either increase or decrease the rate of energy (ATP) production. To better understand the role of aerobic glycolysis for cell growth, we sought to measure directly and precisely the fluxes of O_2 consumption and CO_2 production, and gene regulation (including levels of mRNAs, proteins, and posttranslational modifications) in the conditions of aerobic glycolysis and exponential growth.

RESULTS

Rates of O_2 consumption and CO_2 production have been measured (von Meyenburg, 1969; Verduyn et al., 1991; Van Hoek et al., 1998, 2000; Jouhten et al., 2008; Wiebe et al., 2008) in high-density yeast cultures growing in chemostats at steady state. The most commonly used laboratory growth condition, low-density cultures growing in a batch, however, is a challenging condition for measuring O_2 consumption and CO_2 production because the small number of rapidly growing cells results in small and rapidly changing fluxes. To overcome this challenge and quantify the relative importance of respiration and fermentation during batch cell growth, we developed a bioreactor in which we can accurately measure the absolute rates of O_2 uptake (Ψ_{O_2}) and CO_2 synthesis (Ψ_{CO_2}). In this setup (Figure 1A), a constant flow of air at rate J_{in} containing 20.9% O_2 and 0.04% CO_2 is fed into the bioreactor. By accurately measuring, every second, the O_2 and CO_2 concentrations in the gas leaving the reactor and applying mass conservation (Equations 1 and 2), we can estimate Ψ_{O_2} and Ψ_{CO_2}:

$$\psi_{O_2}(t) = \frac{1}{V_m}\left[J_{in}C_{in}^{O_2} - J_{out}(t)C_{out}^{O_2}(t)\right] \quad \text{(Equation 1)}$$

$$\psi_{CO_2}(t) = \frac{1}{V_m}\left[J_{in}C_{in}^{CO_2} - J_{out}(t)C_{out}^{CO_2}(t)\right] \quad \text{(Equation 2)}$$

The fluxes are normalized to moles per hour by the molar volume V_m of air at $25^{\circ}C$ and 1 atmosphere. The outflow rate (J_{out}) is determined from mass balance analysis and is typically very similar to J_{in}; see Supplemental Information.

To evaluate the accuracy of the O_2 and CO_2 fluxes, we measured these fluxes in control growth conditions for which the molar ratio of CO_2 to O_2, known as respiratory quotient (RQ), is known. First, we grew cells in media containing 100 mM ethanol as a sole source of carbon and energy. The complete oxidation of an ethanol molecule requires three O_2 molecules and produces two CO_2 molecules; thus, chemical stoichiometry and mass conservation require that the RQ for ethanol oxidation equals 2/3, providing a strong benchmark for evaluating the accuracy of our measurements. The measured RQ (Figure 1B) matches the expected value of 2/3. Importantly, the sensitivity of our sensors to very small changes both in O_2 consumption (0.005%) and CO_2 production (0.002%) allows measuring fluxes from low-density yeast cultures (10^5 cells/ml); see Supplemental Information and Figure S1 for details and more control experiments.

Growth Rate and Doubling Time Remain Constant for Nine Doublings

Having established a system for accurate quantification of O_2 and CO_2 fluxes, we applied it to a batch culture of budding yeast; 2 l of well-aerated and well-stirred minimal medium containing 11.11 mM glucose as a sole source of carbon and energy were inoculated to a cell density of 1,000 cells/ml; see Supplemental Information. After 10 hr, the culture reached a cell density allowing bulk measurements and was continuously sampled (Figures 2A and S2). During the first 15 hr of sampling (nine doubling

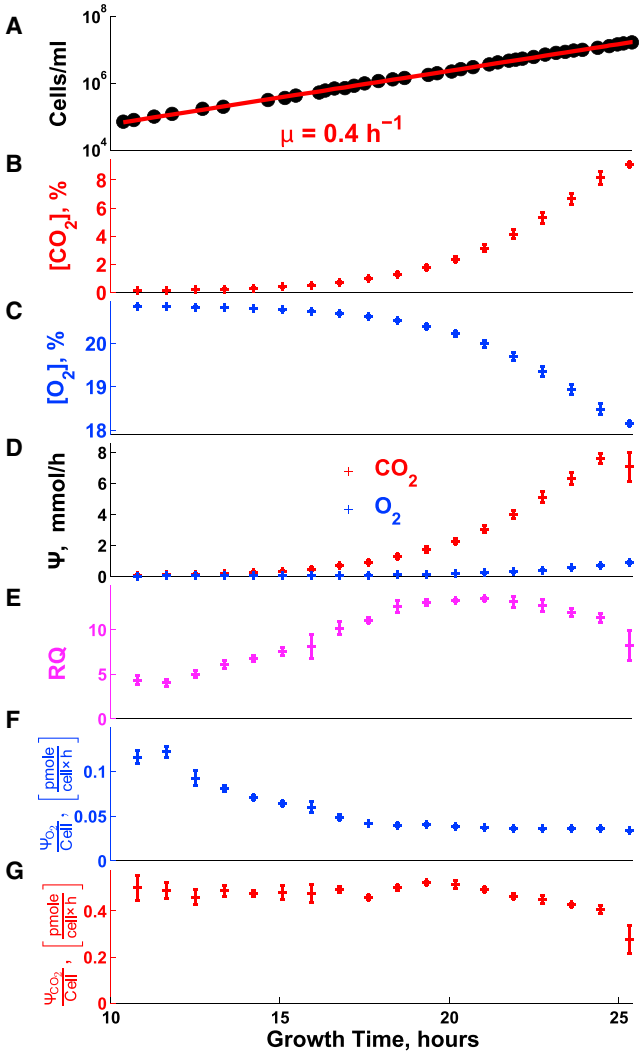

Figure 2. Rates of Respiration and Fermentation Evolve Continuously during Batch Growth at a Constant Growth Rate

(A) Cell density (single cells per ml) during exponential growth on glucose as a sole source of carbon and energy.

(B) The levels of O_2 in the exhaust gas were measured continuously (every second) with a ZrO_2 electrochemical cell.

(C) The levels of CO_2 in the exhaust gas were measured continuously (every second) with infrared spectroscopy.

(D) Fluxes of O_2 uptake (Ψ_{O_2}) and CO_2 production (Ψ_{CO_2}) estimated from the data in (B) and (C) and Equations 1 and 2; see Supplemental Information for details.

(E) Respiratory quotient (RQ), defined as the ratio of Ψ_{CO_2} to Ψ_{O_2}.

(F) Rate of O_2 uptake per cell.

(G) Rate of CO_2 production per cell.

In all panels, error bars denote SDs. See also Figure S2.

periods, the pink region in Figure S2), the cell density increased exponentially with time, indicating a constant rate of cell division (μ = 0.4 hr^{-1}, 1.7 hr doubling time), followed by sudden and complete cessation of growth and division upon glucose exhaustion. Then the cells resumed growth (purple region in Figure S2) supported by the ethanol accumulated during the first growth phase. Notably, during the second growth phase, biomass increased exponentially, indicating again a constant but much slower growth rate μ = 0.04 hr^{-1}. Thus, our experimental design provides two phases of exponential growth, characterized by different carbon sources and growth rates. The transition between the two phases has been studied extensively (Brauer et al., 2005; Zampar et al., 2013), and we will not address it; rather, we focus only on the phases with constant doubling times.

Oxygen Uptake Decreases during Growth at a Constant Rate

The continuously measured concentrations of O_2 and CO_2 (Figures 2B and 2C), and the fluxes estimated from them (Figure 2D), allow computing the RQ during the first phases of exponential growth (Figure 2E). Because the complete oxidation of a glucose molecule requires six O_2 and produces six CO_2, RQ >1 indicates that some glucose is also fermented in the presence of high level of O_2 (Figure 2B), i.e., aerobic glycolysis. Such aerobic glycolysis (RQ >1; Figure 2E) and the exponential growth in Figure 2A are consistent with previous observations (Brauer et al., 2005; Zampar et al., 2013) and expectations. In stark contrast, the continuously changing metabolic fluxes per cell (Figures 2E and 2F) during exponential growth suggest that the cells may not be at steady state even when their growth rate remains constant; this observation is so unexpected that we sought to test it further by multiple independent experimental measurements described below. A second surprising observation is the direction of change: as cells grow and deplete glucose, the oxygen consumption per cell decrease (Figure 2F). This decreasing respiration likely contributes to the cessation of growth after the first growth phase (Figure S2) because cells with downregulated respiration are challenged to grow on ethanol, an obligatory respiratory condition. During the last doublings on glucose, RQ remains high, albeit beginning to decline in concert with CO_2 (Figures 2E and 2G), indicating that the metabolism remains mostly fermentative as long as glucose is present in the medium.

We sought to further test, by independent measurements and mass conservation, the dynamically evolving rates of respiration and fermentation (Figures 2E and 2F) quantified during exponential growth. During the entire first growth phase (Figure 3A), we evaluated whether the flux of carbon intake from glucose equals the sum of all major output carbon fluxes (those due to respiration, biomass synthesis, and fermentation), as required by mass conservation. The results of this mass-balance analysis (Figure 3B) demonstrate that the carbon fluxes estimated from the biomass and the gas measurements account completely and accurately for the fluxes estimated from glucose uptake, thus confirming the accuracy of all measurements and the metabolic dynamics at a constant doubling time.

ATP Production and Stress Resistance Decrease during Exponential Growth

Increasing the rate of aerobic glycolysis is often modeled as a metabolic requirement for increasing the rate of growth (Newsholme et al., 1985; Pfeiffer et al., 2001; Molenaar et al., 2009; Vander Heiden et al., 2009; Vazquez et al., 2010; Shlomi et al., 2011; Lunt and Vander Heiden, 2011; Ward and Thompson, 2012). Because the growth rate remains constant during the

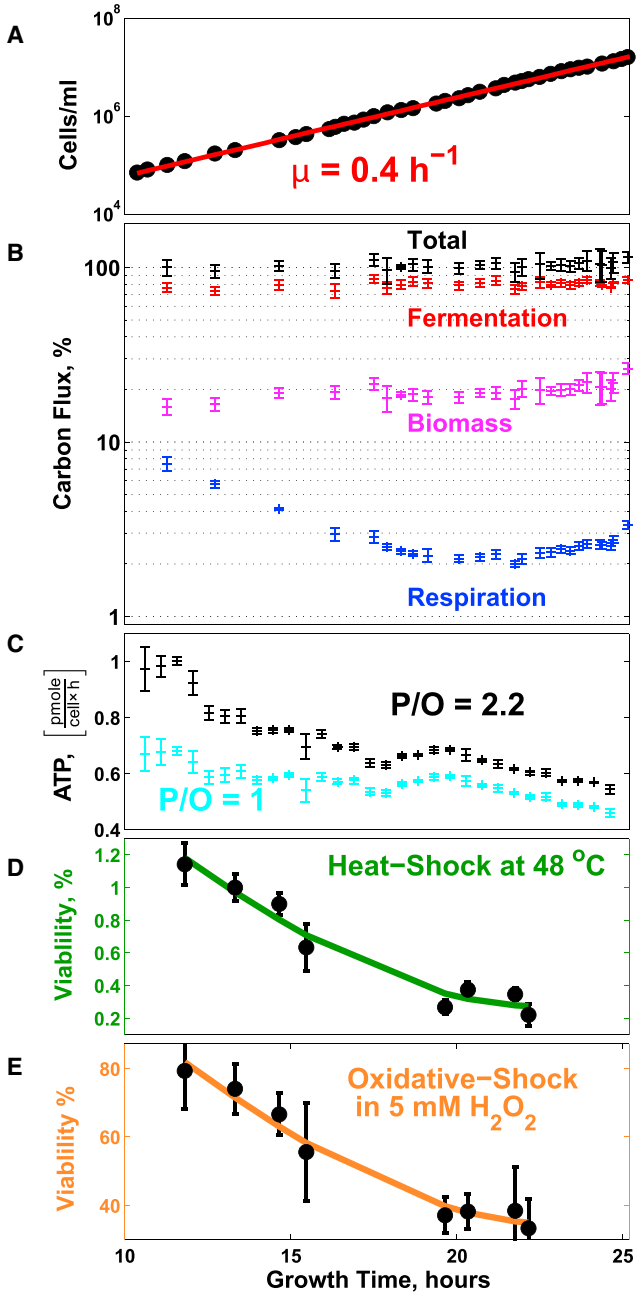

Figure 3. The Fraction of Glucose Carbon Flux Incorporated into Biomass and the Sensitivity to Stress Increase while the Growth Rate Remains Constant

(A) Exponential increase in the number of cells indicates a constant doubling period.

(B) The fraction of carbon flux from glucose (moles of carbon per hour) directed into the major metabolic pathways, as computed from the gas and biomass data, evolves continuously; the sum of the fluxes through these pathways (total) can account, at all time points, for the carbon intake flux from glucose; see Supplemental Information.

(C) The ATP flux was estimated from the fluxes of CO_2 and O_2 in Figures 2E and 2F for low efficiency of oxidative phosphorylation, 1 ATP per oxygen atom (16 ATPs/glucose), and for high efficiency, 2.2 ATPs per oxygen atom (30.4 ATPs/glucose).

(D) The ability of the cells to survive heat shock (48°C for 10 min) declines during the exponential growth phase. Stress sensitivity was quantified by counting colony-forming units (CFUs) on YPD plates.

(E) The ability of the cells to survive oxidative-shock (5 mM H_2O_2 for 10 min) declines during the exponential growth phase.

In all panels, error bars denote SDs. See also Figure S3.

exponential growth phase (Figures 2A and 3A), maximizing growth rate cannot be the only factor accounting for the increasing rate of aerobic glycolysis that we measured (Figures 2E and 3B). Other factors must also influence the rate of aerobic glycolysis.

The reduced oxygen consumption per cell (Figure 2F) and the slight increase in the fraction of glucose carbon directed to biomass synthesis (Figure 3B) suggest a hypothesis, namely, that the increasing rate of aerobic glycolysis might reduce the ATP flux, whereas the cells maintain the same growth rate. To test this hypothesis, we used the O_2 and CO_2 fluxes (Figure 2C) to estimate the rate of ATP production over the range of reported efficiency of oxidative phosphorylation (Hinkle, 2005); see Supplemental Information. The result suggests decreasing rates of total ATP production (Figure 3C), bolstering our hypothesis. The declines in respiration (Figure 2F) and ATP flux (Figure 3C) parallel declines in both heat and oxidative stress resistance (Figures 3D and 3E). In contrast to previous reports (Lu et al., 2009; Zakrzewska et al., 2011), we observe changes in stress resistance, whereas the growth rate remains constant. If the rate of ATP production reflects the cellular energetic demands (Famili et al., 2003), the decreasing ATP flux likely reflects the energy demands associated with respiratory metabolism and stress survival. Thus, the reduced respiration during aerobic glycolysis can reduce the overall rate of energy production (likely reflecting energy demands) in cells maintaining a constant growth rate.

Global Remodeling of Gene Regulation during Exponential Growth

To further evaluate the extent of the metabolic remodeling at a constant doubling period and to identify its molecular basis, we measured the levels of both mRNAs and proteins during the two phases of exponential growth, on glucose or on ethanol (Figure 4). Proteins were labeled with tandem mass tags (TMTs) and quantified by mass spectrometry (MS), resulting in over 58,000 quantified distinct peptides corresponding to over 5,000 proteins at a false discovery rate (FDR) <1%. The peptides where quantified at MS2 level, resulting in high reproducibility (Spearman ρ = 0.993 for swapped TMT labels; Figure S4A) and reliable estimates of fold changes (error <30%) as verified from measuring the levels of the dynamic universal proteomics standard (UPS2) spiked into the yeast samples (Figure S4B). The accuracy of UPS2 fold changes was highest for peptides with low coisolation inferences and thus quantifying proteins based only on peptides with low coisolation improves the accuracy.

During each exponential growth phase, over 1,000 genes (at FDR <1%) increase or decrease monotonically at both the mRNA and the protein levels (Figures 4A and 4B); these genes are highly enriched (Bonferroni corrected p values < 10^{-42}) for

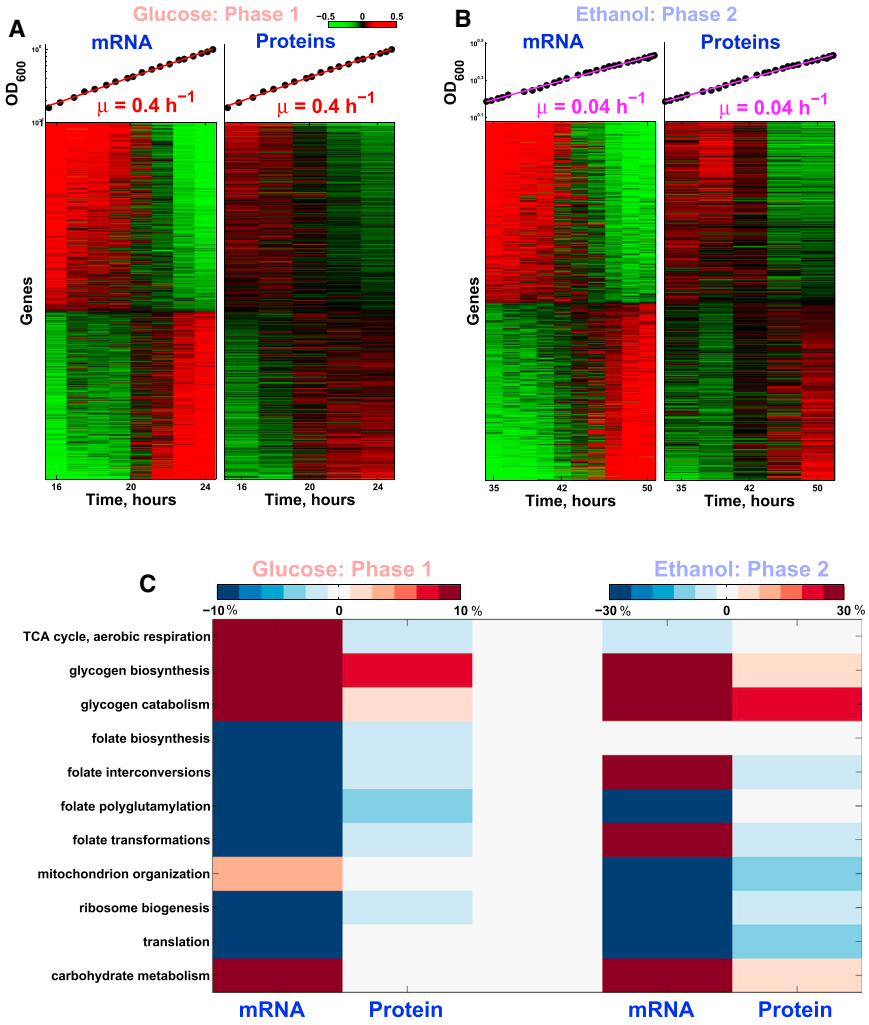

Figure 4. Global Remodeling of mRNA and Protein Regulation during Batch Growth at a Constant Growth Rate

(A) Thousands of mRNAs and proteins (FDR <1%) either increase or decrease monotonically in abundance during the first phase of exponential growth. Levels are reported on a $\log_2$ scale with a 2-fold dynamic range. The mRNA and protein levels were measured in independent (biological replica) cultures, and their correlation reflects the reproducibility of the measurements.

(B) Thousands of mRNAs and proteins (FDR <1%) either increase or decrease monotonically in abundance during the second phase of exponential growth.

(C) Metabolic pathways that show statistically significant dynamics (FDR <1%) during the two phases of exponential growth; see Supplemental Information. The magnitude of change for each gene set is quantified as the average percentage change in the level of its genes per doubling period of the cells.

See also Figure S4.

metabolic and protein synthesis functions (see Supplemental Information), emphasizing the global restructuring of metabolism even as the growth rate remains constant. A decline in protein synthesis genes has been observed previously during the last doubling before glucose exhaustion (Ju and Warner, 1994), and our data show that such decline begins much earlier and continues over many doublings at a constant rate.

Transcription Factors Mediating the Transcriptional Response

The changes in mRNA levels that we measured during exponential growth could reflect two regulatory mechanisms, changes in mRNA production and/or degradation rates. To identify transcription factors (TFs) that mediate some of the changes in the rate of mRNA transcription, we overlapped known TF target genes (MacIsaac et al., 2006) with the sets of genes that either increase or decrease during the first phase of exponential growth (FDR <1%); see Supplemental Information. The results (Table S1) indicate very significant overlap between the genes whose mRNAs decline and the targets of TFs involved in amino acid biogenesis (Gcn4p, Fhl1p, Leu3p, Arg81p, Met4p, and Met32p) and ribosomal biogenesis (Fhl1p, Sfp1p, and Rap1p). The genes whose mRNA levels increase during the exponential growth phase overlap significantly with the targets of TFs regulating cell division (Fkh2p), stress response (Msn2p, and Msn4p), and redox metabolism (Aft1p and Aft2p). The functions and the changing activities of these TFs mirror the transcriptional responses from which they are inferred and add a layer of mechanistic detail to the regulatory dynamics during exponential growth at a constant rate.

Dynamics of Enzymes Regulating Respiratory Metabolism

During the two phases of exponential growth, we systematically compared the dynamic trends in mRNA and protein levels for gene sets defined by all annotated biochemical pathways and by the gene ontology (GO). The statistical significance of the trends within a pathway, quantified by regression slopes, was evaluated by bootstrapping (Airoldi et al., 2009); see Supplemental Information and Figures S4C and S4D for details and all significant genes sets at FDR <1%. Among the pathways exhibiting significant dynamics are gene sets (Figure 4C) mediating the measured changes in metabolic fluxes (Figure 2). The decline in the fraction of aerobically metabolized glucose (Figure 3B) and oxygen consumption (Figure 2F) parallels a decline in the key enzymes that funnel metabolites to respiration. These enzymes include the carnitine shuttle enzymes (Cat2p, Yat1p, and Yat2p) that feed acetyl-CoA to the tricarboxylic acid (TCA) cycle and the rate-regulatory TCA cycle enzymes (Figures 5A and S4)

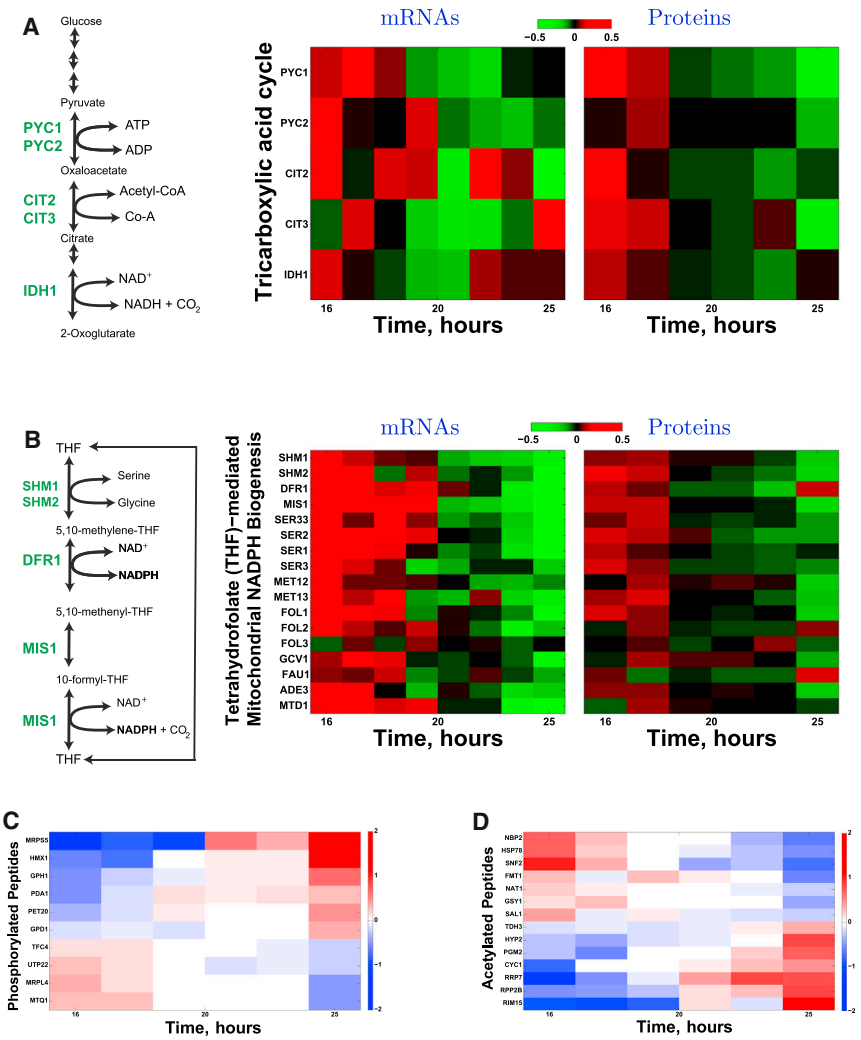

Figure 5. Dynamics of Enzymes and Post-translational Modifications Regulating Respiratory Metabolism at a Constant Growth Rate

(A) The levels of enzymes (and their corresponding mRNAs) catalyzing the first rate-determining reactions of the tricarboxylic acid (TCA) cycle decline, parallel to the decreased oxygen consumption (Figure 2F), during the first exponential growth phase. These enzymes include the pyruvate carboxylases (Pyc1p and Pyc2p), citrate synthetases (Cit1p and Cit2p), and the isocitrate dehydrogenase (Idh1p). See Figures 4 and S4 for other related pathways that also show statistically significant declines. The data are displayed on a $\log_2$ scale with 2-fold dynamical range.

(B) The levels of enzymes (and their corresponding mRNAs) catalyzing the tetrahydrofolate (THF)-mediated mitochondrial NADPH biogenesis decline, parallel to the decreased oxygen consumption (Figure 2F), during the first exponential growth phase. These include all enzymes (Ser3p, Ser33p, Ser1p, and Ser2p) catalyzing the serine biosynthesis from 3-phosphoglycerate, the hydroxymethyltransferases (Shm1p and Shm2p) and the mitochondrial NADPH synthetases: the dihydrofolate reductase (Dfr1p) and the mitochondrial C1-tetrahydrofolate synthase (Mis1p). See Figures 4 and S4 for other related pathways that also show statistically significant declines. The data are displayed on a $\log_2$ scale with 2-fold dynamical range.

(C) Levels of phosphorylated peptides change during exponential growth at a constant rate.

(D) Levels of acetylated peptides change during exponential growth at a constant rate. The levels of peptides with posttranslational modifications are shown on a $\log_2$ scale, and the corresponding proteins are marked on the y axis.

See also Figure S5.

that catalyze the reactions through which metabolites enter the TCA. The levels of some mRNAs coding for TCA enzymes also decrease, whereas the levels of other mRNAs coding for TCA enzymes increase (Figure S5A). The levels of mRNAs coding for the initial and flux-regulatory TCA enzymes decline in concert with the corresponding proteins, including pyruvate carboxylase (PYC) isoforms 1 and 2, citrate synthetases 2 and 3, and the isocitrate dehydrogenase 1 (Figure 5A). Another transcriptional reflection of the decreased respiration during phase 1 is the decline of the mRNAs for the glutathione-dependent oxidoreductases (*GRX3* and *GRX4*; Figure S5B), whose transcription is sensitive to peroxide and superoxide radicals (Pujol-Carrion et al., 2006).

The mitochondrial respiratory chain generates reactive oxygen species (ROS) whose neutralization requires tetrahydrofolate (THF)-mediated mitochondrial NADPH production from the carbon 3 of serine by the reactions shown in Figure 5B (Appling, 1991; García-Martínez and Appling, 1993). All enzymes (and their corresponding mRNAs) producing NADPH from these pathways and from the associated pathways (Figures 5B and S4) decline in parallel with the declining oxygen consumption (Figure 2) during the exponential growth phase. This concerted decline is particularly pronounced for the mitochondrial enzymes (Dfr1p and Mis1p) catalyzing the NADPH generating reactions (Figure 5B). The decline also includes all enzymes (Ser3p, Ser33p, Ser1p, and Ser2p) catalyzing the serine biosynthesis from 3-phosphoglycerate. Because the growth rate and the cytoplasmic serine concentration remain constant (Figure S5C), the declining levels of serine biosynthetic enzymes likely reflect a decreasing flux of serine toward the folate-mediated mitochondrial NADPH production. Such a decrease in NADPH production could explain at least in part the decreased stress resistance that we measured (Figures 3D and 3E). This pathway for THF-mediated mitochondrial NADPH production is transcriptional upregulated with the growth rate and increased respiration of yeast growing on ethanol carbon source (Slavov and Botstein, 2011), suggesting its broader significance for respiratory metabolism.

Similarly, pervasive dynamics in metabolic pathways are observed during the second phase of exponential growth (Figure 4C and Figure S4C). The changing levels of metabolic enzymes synthesizing amino acids during the two exponential

phases also lead to concerted changes in the intracellular amino acid levels (Figure S5C).

Posttranslational Modifications during Exponential Growth

Hundreds of peptides quantified by MS carried posttranslational modifications (PTMs), such as phosphorylation (of Ser and Thr) and acetylation (of Lys and Arg). Similar to the metabolic fluxes, mRNA and protein levels, the levels of peptides with PTMs increase or decrease over 10-fold dynamic range (Figures 5C, 5D, and S5D) during the exponential growth phases. These PTM dynamics reinforce the regulatory dynamics suggested by the metabolic fluxes, mRNAs, and proteins levels (Figures 4A and 4B). For example, the decreasing fraction of glucose carbon directed toward respiration is associated with the phosphorylation of the pyruvate dehydrogenase (Pda1p) that regulates the balance between respiration and fermentation and the acetylation of the glycolytic enzyme glyceraldehyde-3-phosphate dehydrogenase (Tdh3p). Furthermore, the reduced respiration per cell (Figure 2F) is reflected in the phosphorylation pattern (Figure 5C) of mitochondrial respiratory and heme-related proteins (Pet20p and Hmx1p), of mitochondrial ribosomal proteins (Mrps5p and Mrpl4p), and the acetylation pattern (Figure 5D) of Cytochrome c (Cyc1p). The increasing metabolism of reserved carbohydrates during the first growth phase indicated by the mRNA and protein trends (Figures 4A–4C and S4) is also detected in the PTMs of participating enzymes (Gph1p and Pgm2p). Similarly, the translation-related changes in gene regulation (Figures 4A–4C and S4) are paralleled by translation-related PTMs including proteins involved in rRNA maturation and ribosome biogenesis (Utp22p and Rrp7p), elongation-related factors (Hyp2p, Rpp2bp, and Mtq1p), and tRNA synthesis (Tfc4p). Other proteins with dynamic PTMs during exponential growth (Figures 5C and 5D) include the proliferation regulating kinase Rim15p, the acetyltransferase (Nat1p), and the methyltransferase (Mtq1p), suggesting crosstalk among PTM signaling pathways. These results imply that quantifying PTM dynamics during well-characterized physiological states is a promising direction for characterizing the vast and largely unexplored space of PTM functions.

DISCUSSION

Six independent measurements (respiration, stress resistance, transcripts, proteins, amino acids, and PTMs) demonstrate that metabolism, gene regulation, and stress sensitivity can change substantially even when the doubling time does not change over nine generations. Specifically, we found that, as aerobic glycolysis increases, a constant rate of biomass synthesis can be sustained with decreasing rate of ATP production. In other words, cells with reduced rate of respiration are able to maintain their growth rate constant with lower total ATP flux. Thus, if the rate of ATP production reflects the cellular energy demands (Famili et al., 2003), our data suggest that although respiration is efficient in generating ATP, it may also substantially increase the energetic demands for growth, even when growth rate remains constant for many generations. Therefore, aerobic glycolysis may reduce the energetic demands of cellular growth by reducing the energy associated with respiration, such as that needed for detoxification of reactive oxygen species. Such decreased oxidative-stress defenses can naturally explain the decreasing stress resistance that we measured in the course of exponential growth at a constant rate.

The decreasing rate of ATP production with the shift toward less aerobic metabolism prompts the reevaluation of the current estimates for the efficiency of oxidative phosphorylation based on the assumption that yeast growing in aerobic and in anaerobic conditions have identical energy requirements (von Meyenburg, 1969; Verduyn et al., 1991; Famili et al., 2003). The decreased respiration in our cultures coincides with a concerted downregulation, at both the mRNA and protein levels, of the TCA enzymes regulating the entry of metabolites into the respiratory pathway. This downregulation of rate-determining enzymes not only supports the measured decrease in oxygen consumption but also suggests the molecular mechanisms mediating it. Similarly, we found that all pathways associated with the tetrahydrofolate-mediated production of mitochondrial NADPH decline in parallel to the decreased oxygen consumption and the decreased stress resistance, emphasizing the ROS burden of respiratory metabolism and the role of mitochondrial NADPH for relieving it.

Most work on aerobic glycolysis has focused on the correlation between aerobic glycolysis and growth rate (Warburg, 1956; Newsholme et al., 1985; De Deken, 1966; Brand and Hermfisse, 1997; Pfeiffer et al., 2001; Bauer et al., 2004; Gatenby and Gillies, 2004; Molenaar et al., 2009; Vander Heiden et al., 2009; Vazquez et al., 2010; Shlomi et al., 2011; Lunt and Vander Heiden, 2011; Ward and Thompson, 2012). However, there are also examples of decoupling aerobic glycolysis and growth rate. These examples include high rates of fermentation measured in slowly growing yeast whose growth is limited by auxotrophic nutrients (Boer et al., 2008; Slavov and Botstein, 2013) and in quiescent mammalian fibroblasts whose growth is inhibited by serum withdrawal and/or contact inhibition (Lemons et al., 2010). Our data and analysis build upon and expand previous work showing decoupling of aerobic glycolysis and cellular growth rate in several ways: (1) measurements of oxygen consumption (Figure 2), (2) estimation of the total rate of ATP production (Figure 3), (3) demonstration that the measured flux of carbon intake equals the measured flux of carbon release (Figure 3), (4) measurements of stress resistance (Figure 3), and (5) measurements of protein levels and PTMs (Figures 4 and 5). The measurement of oxygen consumption allows quantifying the extent of aerobic glycolysis by the respiratory quotient, and the carbon flux balance provides a cross-check of all measurements. Thus, we can rule out the possibility that our results are influenced by unmeasured fluxes, such as respiration, or by incorrectly measured fluxes. Our results are also unlikely to be influenced by mutations and external perturbations because our measurements were performed in wild-type cells growing in very well-defined conditions. The estimate of energy production indicates that cells can support a constant growth rate while decreasing the rate of energy production and increasing the rate of aerobic glycolysis. Our results are consistent with and add to previous work (Brand and Hermfisse, 1997; Lemons et al., 2010; Jain et al., 2012; Chang et al., 2013)

pointing to roles of aerobic glycolysis beyond maximizing cellular growth rate. Therefore, we conclude that understanding aerobic glycolysis requires taking into account multiple aspects of aerobic metabolism, such as mitochondrial NADPH production, not just the growth rate.

Many researchers (Ju and Warner, 1994; Shachrai et al., 2010; Zampar et al., 2013; Bren et al., 2013) have reported dynamic changes during batch growth. To our knowledge, all previous reports were confined either to nonexponentially growing cultures or to a single exogenous protein or to the last generation of batch growth when growth rate, to the extent it can estimated, was declining. In contrast, we observed pervasive dynamics during the whole span (including early and middle phases) of batch growth, including during phases that are considered to represent a single well-defined steady state (Newman et al., 2006; Belle et al., 2006; Pelechano and Pérez-Ortín, 2010; Schwanhäusser et al., 2011; Heyland et al., 2009; Youk and van Oudenaarden, 2009; Boisvert et al., 2012).

Our data demonstrate that, at least for two very different growth conditions, exponentially growing cultures can change their metabolism continuously, prompting the investigation of metabolic and cell-signaling dynamics even in conditions previously assumed to represent steady states (Silverman et al., 2010; Slavov et al., 2011, 2013). However, our data do not suggest that all exponentially growing cultures change their metabolism continuously and steady state is impossible; many examples document constant, steady-state fluxes in exponentially growing cultures (von Meyenburg, 1969; Küenzi and Fiechter, 1969; Van Hoek et al., 2000; Brauer et al., 2005, 2008; Slavov and Botstein, 2011, 2013). Our finding of changing metabolism and cell physiology at a constant growth rate provides a new direction for studying physiological dynamics and tradeoffs, such as allowing flux-balance models to account for a constant growth rate at varying glucose uptake rates.

EXPERIMENTAL PROCEDURES

All experiments described in the paper used a prototrophic diploid strain (DBY12007) with a S288c background and wild-type HAP1 alleles, MATa/MATα *HAP* 1^+. We grew our cultures in a commercial bioreactor (LAMBDA Laboratory Instruments), using minimal media with the composition of yeast nitrogen base (YNB) supplemented with 2 g/l D-glucose. CO_2 and O_2 were measured, every second, in the off-gas with zirconia and infrared sensors, respectively. All other measurements were done on samples taken from the culture via a sterile sampling port. Cell density was measured by a Coulter counter counting of at least 20,000 cells (Slavov et al., 2011; Bryan et al., 2012). Stress sensitivity was assayed (Slavov et al., 2012) by exposing 250 μl culture to stress for 10 min and subsequent plating on YPD plates to count colony forming units (survived cells). Details for all measurements and quality controls can be found in the Supplemental Information.

ACCESSION NUMBERS

The GEO accession number for the gene expression data reported herein is GSE56773.

SUPPLEMENTAL INFORMATION

Supplemental Information includes Supplemental Experimental Procedures, five figures, one table, and one data file and can be found with this article online at http://dx.doi.org/10.1016/j.celrep.2014.03.057.

ACKNOWLEDGMENTS

We thank S. Manalis for the use of his Coulter counter and K. Chatman for assistance with measuring amino acid levels, as well as J. Rabinowitz, D. Botstein, N. Wingreen, A. Murray, Q. Justman, E. Solis, and members of the van Oudenaarden lab for critical discussions. This work was funded by grants from the NIH to A.v.O. (DP1 CA174420, R01-GM068957, and U54CA143874) and E.M.A. (R01-GM-096193) and an Alfred P. Sloan Research Fellowship to E.M.A.

Received: November 18, 2013
Revised: February 11, 2014
Accepted: March 21, 2014
Published: April 24, 2014

REFERENCES

Airoldi, E.M., Huttenhower, C., Gresham, D., Lu, C., Caudy, A., Dunham, M., Broach, J., Botstein, D., and Troyanskaya, O.G. (2009). Predicting cellular growth from gene expression signatures. PLoS Comput. Biol., e1000257.

Appling, D.R. (1991). Compartmentation of folate-mediated one-carbon metabolism in eukaryotes. FASEB J. *5*, 2645–2651.

Bauer, D.E., Harris, M.H., Plas, D.R., Lum, J.J., Hammerman, P.S., Rathmell, J.C., Riley, J.L., and Thompson, C.B. (2004). Cytokine stimulation of aerobic glycolysis in hematopoietic cells exceeds proliferative demand. FASEB J. *18*, 1303–1305.

Belle, A., Tanay, A., Bitincka, L., Shamir, R., and O'Shea, E.K. (2006). Quantification of protein half-lives in the budding yeast proteome. Proc. Natl. Acad. Sci. USA *103*, 13004–13009.

Boer, V.M., Amini, S., and Botstein, D. (2008). Influence of genotype and nutrition on survival and metabolism of starving yeast. Proc. Natl. Acad. Sci. USA *105*, 6930–6935.

Boisvert, F.-M., Ahmad, Y., Gierliński, M., Charrière, F., Lamont, D., Scott, M., Barton, G., and Lamond, A.I. (2012). A quantitative spatial proteomics analysis of proteome turnover in human cells. Mol. Cell. Proteomics *11*, 011429.

Brand, K.A., and Hermfisse, U. (1997). Aerobic glycolysis by proliferating cells: a protective strategy against reactive oxygen species. FASEB J. *11*, 388–395.

Brauer, M.J., Saldanha, A.J., Dolinski, K., and Botstein, D. (2005). Homeostatic Adjustment and Metabolic Remodeling in Glucose-limited Yeast Cultures. Molecular Biology of the Cell *16*, 2503–2517, 19.

Brauer, M.J., Huttenhower, C., Airoldi, E.M., Rosenstein, R., Matese, J.C., Gresham, D., Boer, V.M., Troyanskaya, O.G., and Botstein, D. (2008). Coordination of growth rate, cell cycle, stress response, and metabolic activity in yeast. Mol. Biol. Cell *19*, 352–367.

Bren, A., Hart, Y., Dekel, E., Koster, D., and Alon, U. (2013). The last generation of bacterial growth in limiting nutrient. BMC Syst. Biol. *7*, 27.

Bryan, A.K., Engler, A., Gulati, A., and Manalis, S.R. (2012). Continuous and long-term volume measurements with a commercial Coulter counter. PLoS ONE *7*, e29866.

Campbell, S.L., Jones, K.A., and Shulman, R.G. (1985). In vivo 31P nuclear magnetic resonance saturation transfer measurements of phosphate exchange reactions in the yeast Saccharomyces cerevisiae. FEBS Lett. *193*, 189–193.

Chang, C.-H., Curtis, J.D., Maggi, L.B., Jr., Faubert, B., Villarino, A.V., O'Sullivan, D., Huang, S.C., van der Windt, G.J., Blagih, J., Qiu, J., et al. (2013). Posttranscriptional control of T cell effector function by aerobic glycolysis. Cell *153*, 1239–1251.

Clasquin, M.F., Melamud, E., Singer, A., Gooding, J.R., Xu, X., Dong, A., Cui, H., Campagna, S.R., Savchenko, A., Yakunin, A.F., et al. (2011). Riboneogenesis in yeast. Cell *145*, 969–980.

De Deken, R.H. (1966). The Crabtree effect: a regulatory system in yeast. J. Gen. Microbiol. *44*, 149–156.

DeBerardinis, R.J., Mancuso, A., Daikhin, E., Nissim, I., Yudkoff, M., Wehrli, S., and Thompson, C.B. (2007). Beyond aerobic glycolysis: transformed cells can

engage in glutamine metabolism that exceeds the requirement for protein and nucleotide synthesis. Proc. Natl. Acad. Sci. USA *104*, 19345–19350.

Famili, I., Förster, J., Nielsen, J., and Palsson, B.O. (2003). Saccharomyces cerevisiae phenotypes can be predicted by using constraint-based analysis of a genome-scale reconstructed metabolic network. Proc. Natl. Acad. Sci. USA *100*, 13134–13139.

García-Martínez, L.F., and Appling, D.R. (1993). Characterization of the folate-dependent mitochondrial oxidation of carbon 3 of serine. Biochemistry *32*, 4671–4676.

Gatenby, R.A., and Gillies, R.J. (2004). Why do cancers have high aerobic glycolysis? Nat. Rev. Cancer *4*, 891–899.

Gyulai, L., Roth, Z., Leigh, J.S., Jr., and Chance, B. (1985). Bioenergetic studies of mitochondrial oxidative phosphorylation using 31phosphorus NMR. J. Biol. Chem. *260*, 3947–3954.

Hanahan, D., and Weinberg, R.A. (2011). Hallmarks of cancer: the next generation. Cell *144*, 646–674.

Hartwell, L.H., Hopfield, J.J., Leibler, S., and Murray, A.W. (1999). From molecular to modular cell biology. Nature *402* (6761, Suppl), C47–C52.

Heyland, J., Fu, J., and Blank, L.M. (2009). Correlation between TCA cycle flux and glucose uptake rate during respiro-fermentative growth of Saccharomyces cerevisiae. Microbiology *155*, 3827–3837.

Hinkle, P. (2005). P/O ratios of mitochondrial oxidative phosphorylation. Biochimica et Biophysica Acta (BBA)-. Bioenergetics *1706*, 1–11.

Jain, M., Nilsson, R., Sharma, S., Madhusudhan, N., Kitami, T., Souza, A.L., Kafri, R., Kirschner, M.W., Clish, C.B., and Mootha, V.K. (2012). Metabolite profiling identifies a key role for glycine in rapid cancer cell proliferation. Science *336*, 1040–1044.

Jouhten, P., Rintala, E., Huuskonen, A., Tamminen, A., Toivari, M., Wiebe, M., Ruohonen, L., Penttilä, M., and Maaheimo, H. (2008). Oxygen dependence of metabolic fluxes and energy generation of Saccharomyces cerevisiae CEN.PK113-1A. BMC Syst. Biol. *2*, 60.

Ju, Q., and Warner, J.R. (1994). Ribosome synthesis during the growth cycle of Saccharomyces cerevisiae. Yeast *10*, 151–157.

Krebs, H.A., and Eggleston, L.V. (1940). The oxidation of pyruvate in pigeon breast muscle. Biochem. J. *34*, 442–459.

Küenzi, M.T., and Fiechter, A. (1969). Changes in carbohydrate composition and trehalase-activity during the budding cycle of Saccharomyces cerevisiae. Arch. Mikrobiol. *64*, 396–407.

Lemons, J.M.S., Feng, X.J., Bennett, B.D., Legesse-Miller, A., Johnson, E.L., Raitman, I., Pollina, E.A., Rabitz, H.A., Rabinowitz, J.D., and Coller, H.A. (2010). Quiescent fibroblasts exhibit high metabolic activity. PLoS Biol. *8*, e1000514.

Lu, C., Brauer, M.J., and Botstein, D. (2009). Slow growth induces heat-shock resistance in normal and respiratory-deficient yeast. Mol. Biol. Cell *20*, 891–903.

Lunt, S.Y., and Vander Heiden, M.G. (2011). Aerobic glycolysis: meeting the metabolic requirements of cell proliferation. Annu. Rev. Cell Dev. Biol. *27*, 441–464.

MacIsaac, K.D., Wang, T., Gordon, D.B., Gifford, D.K., Stormo, G.D., and Fraenkel, E. (2006). An improved map of conserved regulatory sites for Saccharomyces cerevisiae. BMC Bioinformatics *7*, 113.

McKnight, S.L. (2010). On getting there from here. Science *330*, 1338–1339.

Molenaar, D., van Berlo, R., de Ridder, D., and Teusink, B. (2009). Shifts in growth strategies reflect tradeoffs in cellular economics. Mol. Syst. Biol. *5*, 323.

Monod, J. (1949). The Growth of Bacterial Cultures. Annu. Rev. Microbiol. *3*, 371–394.

Newman, J.R., Ghaemmaghami, S., Ihmels, J., Breslow, D.K., Noble, M., DeRisi, J.L., and Weissman, J.S. (2006). Single-cell proteomic analysis of S. cerevisiae reveals the architecture of biological noise. Nature *441*, 840–846.

Newsholme, E.A., Crabtree, B., and Ardawi, M.S. (1985). The role of high rates of glycolysis and glutamine utilization in rapidly dividing cells. Biosci. Rep. *5*, 393–400.

Pelechano, V., and Pérez-Ortín, J.E. (2010). There is a steady-state transcriptome in exponentially growing yeast cells. Yeast *27*, 413–422.

Pfeiffer, T., Schuster, S., and Bonhoeffer, S. (2001). Cooperation and competition in the evolution of ATP-producing pathways. Science *292*, 504–507.

Portman, M.A. (1994). Measurement of unidirectional $P_i \rightarrow ATP$ flux in lamb myocardium *in vivo*. Biochim. Biophys. Acta *1185*, 221–227.

Pujol-Carrion, N., Belli, G., Herrero, E., Nogues, A., and de la Torre-Ruiz, M.A. (2006). Glutaredoxins Grx3 and Grx4 regulate nuclear localisation of Aft1 and the oxidative stress response in Saccharomyces cerevisiae. J. Cell Sci. *119*, 4554–4564.

Rich, P.R. (2003). The molecular machinery of Keilin's respiratory chain. Biochem. Soc. Trans. *31*, 1095–1105.

Schwanhäusser, B., Busse, D., Li, N., Dittmar, G., Schuchhardt, J., Wolf, J., Chen, W., and Selbach, M. (2011). Global quantification of mammalian gene expression control. Nature *473*, 337–342.

Scott, M., Gunderson, C.W., Mateescu, E.M., Zhang, Z., and Hwa, T. (2010). Interdependence of cell growth and gene expression: origins and consequences. Science *330*, 1099–1102.

Shachrai, I., Zaslaver, A., Alon, U., and Dekel, E. (2010). Cost of unneeded proteins in *E. coli* is reduced after several generations in exponential growth. Mol. Cell *38*, 758–767.

Sheldon, J.G., Williams, S.P., Fulton, A.M., and Brindle, K.M. (1996). 31P NMR magnetization transfer study of the control of ATP turnover in Saccharomyces cerevisiae. Proc. Natl. Acad. Sci. USA *93*, 6399–6404.

Shlomi, T., Benyamini, T., Gottlieb, E., Sharan, R., and Ruppin, E. (2011). Genome-scale metabolic modeling elucidates the role of proliferative adaptation in causing the Warburg effect. PLoS Comput. Biol. *7*, e1002018.

Silverman, S.J., Petti, A.A., Slavov, N., Parsons, L., Briehof, R., Thiberge, S.Y., Zenklusen, D., Gandhi, S.J., Larson, D.R., Singer, R.H., and Botstein, D. (2010). Metabolic cycling in single yeast cells from unsynchronized steady-state populations limited on glucose or phosphate. Proc. Natl. Acad. Sci. USA *107*, 6946–6951.

Slavov, N., and Botstein, D. (2011). Coupling among growth rate response, metabolic cycle, and cell division cycle in yeast. Mol. Biol. Cell *22*, 1997–2009.

Slavov, N., and Botstein, D. (2013). Decoupling nutrient signaling from growth rate causes aerobic glycolysis and deregulation of cell size and gene expression. Mol. Biol. Cell *24*, 157–168.

Slavov, N., Macinskas, J., Caudy, A., and Botstein, D. (2011). Metabolic cycling without cell division cycling in respiring yeast. Proc. Natl. Acad. Sci. USA *108*, 19090–19095.

Slavov, N., Airoldi, E.M., van Oudenaarden, A., and Botstein, D. (2012). A conserved cell growth cycle can account for the environmental stress responses of divergent eukaryotes. Mol. Biol. Cell *23*, 1986–1997.

Slavov, N., Carey, J., and Linse, S. (2013). Calmodulin transduces Ca2+ oscillations into differential regulation of its target proteins. ACS Chem. Neurosci. *4*, 601–612.

Van Hoek, P., Van Dijken, J.P., and Pronk, J.T. (1998). Effect of specific growth rate on fermentative capacity of baker's yeast. Appl. Environ. Microbiol. *64*, 4226–4233.

Van Hoek, P., van Dijken, J.P., and Pronk, J.T. (2000). Regulation of fermentative capacity and levels of glycolytic enzymes in chemostat cultures of Saccharomyces cerevisiae. Enzyme Microb. Technol. *26*, 724–736.

Vander Heiden, M.G., Cantley, L.C., and Thompson, C.B. (2009). Understanding the Warburg effect: the metabolic requirements of cell proliferation. Science *324*, 1029–1033.

Vazquez, A., Liu, J., Zhou, Y., and Oltvai, Z.N. (2010). Catabolic efficiency of aerobic glycolysis: the Warburg effect revisited. BMC Syst. Biol. *4*, 58.

Verduyn, C., Stouthamer, A.H., Scheffers, W.A., and van Dijken, J.P. (1991). A theoretical evaluation of growth yields of yeasts. Antonie van Leeuwenhoek *59*, 49–63.

von Meyenburg, K.H. (1969). Energetics of the budding cycle of *Saccharomyces cerevisiae* during glucose limited aerobic growth. Arch. Mikrobiol. *66*, 289–303.

Warburg, O. (1956). On respiratory impairment in cancer cells. Science *124*, 269–270.

Ward, P.S., and Thompson, C.B. (2012). Metabolic reprogramming: a cancer hallmark even warburg did not anticipate. Cancer Cell *21*, 297–308.

Wiebe, M.G., Rintala, E., Tamminen, A., Simolin, H., Salusjärvi, L., Toivari, M., Kokkonen, J.T., Kiuru, J., Ketola, R.A., Jouhten, P., et al. (2008). Central carbon metabolism of Saccharomyces cerevisiae in anaerobic, oxygen-limited and fully aerobic steady-state conditions and following a shift to anaerobic conditions. FEMS Yeast Res. *8*, 140–154.

Youk, H., and van Oudenaarden, A. (2009). Growth landscape formed by perception and import of glucose in yeast. Nature *462*, 875–879.

Zakrzewska, A., van Eikenhorst, G., Burggraaff, J.E., Vis, D.J., Hoefsloot, H., Delneri, D., Oliver, S.G., Brul, S., and Smits, G.J. (2011). Genome-wide analysis of yeast stress survival and tolerance acquisition to analyze the central trade-off between growth rate and cellular robustness. Mol. Biol. Cell *22*, 4435–4446.

Zampar, G.G., Kümmel, A., Ewald, J., Jol, S., Niebel, B., Picotti, P., Aebersold, R., Sauer, U., Zamboni, N., and Heinemann, M. (2013). Temporal system-level organization of the switch from glycolytic to gluconeogenic operation in yeast. Mol. Syst. Biol. *9*, 651.

SUPPLEMENTAL INFORMATION

Constant Growth Rate Can Be Supported by Decreasing Energy Flux and Increasing Aerobic Glycolysis

Nikolai Slavov,* Bogdan A. Budnik, David Schwab, Edoardo M. Airoldi, and Alexander van Oudenaarden*

*Correspondence: nslavov@alum.mit.edu (N.S.) or a.vanoudenaarden@hubrecht.eu (A.v.O)

Experimental Design

All experiments described in the paper used a prototrophic diploid strain (DBY12007) with a S288c background and wild type HAP1 alleles, MAT**a**/MATα $HAP1^{+}$, first derived by Hickman and Winston (2007). We grew our cultures in a commercial bioreactor (LAMBDA Laboratory Instruments) using minimal media with the composition of yeast nitrogen base (YNB) and supplemented with $2g/L$ D-glucose. Before inoculation, the reactor was filled with 2L of minimal media warmed up to a working temperature of $30^{o}C$ and after reaching a steady-state of temperature and media aeration for a few hours, the oxygen and the carbon dioxide sensors were calibrated. After calibration, oxygen and the carbon dioxide data were collected for at least 3 hours to ensure that the readings were stable, not changing.

Then cultures were started by inoculating the media with 100 μl overnight culture from DBY12007. The overnight cultures were prepared by first streaking frozen DBY12007 on YPD plates (YPD; 10 g of Bacto-Yeast extract, 20 g of Bacto-peptone, 20 g of Bacto-agar, and 20 g of glucose in 1000 ml of water) and then growing a single colony in the same minimal media used for the subsequent growth experiment in the bioreactor. The density of the culture used for inoculation was 2×10^{7} cells per ml, resulting in initial density of 10^{3} cells/ml for the culture in the reactor. The cultures were grown at $30^{o}C$ and continuously stirred to ensure their homogeneity. The culture was aerated

with air coming from a compressed gas cylinder (Airgas, AI-B300 breathable air). The incoming flow of air was controlled by a thermal-based mass-flow controller and filtered through a $0.2\mu m$ filter to ensure sterility.

Sampling

To take samples without disturbing the cultures, we used a metal tube attached to a silicon tubing and a syringe. The metal tube could be inserted in and out of the cultures, and the syringe used to sample the required volume quickly from the homogeneous cultures. The sampling tubing was kept sterile and no culture was left in it after sampling. The volume of each sample was recorded and taken into account as necessary for estimating metabolic rates on a per cell basis. All samples were immediately processed as described in the subsections below.

Measuring of Culture Biomass

We used 3 methods to measure biomass. A single cell measurement of cell density was performed on Beckman-Coulter Multisizer 4 by counting of at least 20,000 single cells (Slavov et al., 2011; Bryan et al., 2012). Biomass density was also measured by the optical density at 600 nm (OD600) on a Hitachi U-1800 spectrophotometer and by measuring the grams of dry weight (gDW) of yeast cells. For dry weight measurements, culture samples (between 10 and 50 ml depending on cell density) were filtered through pre-weighed filters (pore size of 0.22 μm). The filters with the cells were dried in a microwave oven and weighed every 5 min until the weight stabilized. The gDW/ml is estimated as the difference in the weight of the filter with and without the dried cells normalized to the volume of the filtered culture.

Two liters of well-aerated and well-stirred minimal medium containing 11.11 mM glucose as a sole source of carbon and energy were inoculated to a cell density of 1000 cells/ml (Figure 1A). After 10 hours (h), the culture reached a cell density allowing bulk measurements and was continuously sampled. During the first 10 h of sampling (6 doubling periods, the pink region in Figure S2A-B), the biomass and the cell density increased exponentially with time, indicating a

constant growth rate ($\mu = 0.4\ \ h^{-1}$) and cell division cycle (CDC) period ($1.7\ h$). Subsequently, the CDC period remained constant at $1.7\ h$ for 3 more doublings while cell-size and thus growth rate declined, dark pink region in Figure S2A-B. In fact, the doubling time remained constant until the median cell volume dropped by 3-fold and both cell growth and division stopped suddenly and completely (Figure S2C). Then the cells resumed growth (purple region in Figure S2A-B) supported by the ethanol accumulated during the first growth phase. Notably, during the second growth phase, biomass increased exponentially, indicating again a constant but much slower growth rate $\mu = 0.04\ h^{-1}$. Thus, our experimental design provides two phases of exponential growth, characterized by different carbon sources and growth rates. The transition between the two phases has been studied extensively (Brauer et al., 2005; Zampar et al., 2013) and we will not address it; rather, we focus only on the phases with constant doubling times.

Estimating O_2 Consumption and CO_2 Production

The schematic diagram for measuring oxygen consumption and carbon dioxide production is shown in Figure 1A. The air aerating the culture comes from a compressed-air bottle and has known concentrations of carbon dioxide ($C_{in}^{CO_2} = 0.04\%$) and of oxygen ($C_{in}^{O_2} = 20.94\%$). The remainder is nitrogen ($C_{in}^{N_2} = 78.08\%$), argon ($C_{in}^{Ar} = 0.93\%$) and trace gases (mostly neon) below 0.002%. We can set the rate of air entering the culture (J_{in}, $[L/h]$) and measure the concentrations of carbon dioxide (using infra-red spectroscopy) and of oxygen (using zirconia galvanic cell) leaving the reactor every second during the experiment, $C_{out}^{CO_2}(t)$ and $C_{out}^{O_2}(t)$ respectively. Based on these data and using mass-conservation, we want to estimate the rate of O_2 consumption and the rate of CO_2 production.

Estimating the Off-gas Flux

Because the volume of produced CO_2 can be different from the volume of consumed O_2, the total volume of the gas leaving the reactor per second can be slightly smaller or larger than the total volume entering the reactor per second. Since yeast do not consume or produce argon and nitrogen, we can use our measurements to compute the flux of air leaving the reactor every second, $J_{out}(t)$, as follows:

- The concentration of the inert gases (nitrogen and argon) in the incoming air is: $C_{in}^{inert} = 100 - C_{in}^{CO_2} - C_{in}^{O_2} = C_{in}^{Ar} + C_{in}^{N_2} = 0.9\% + 78.08\% = 78.98\%$.

- The concentration of the inert gases (nitrogen and argon) in the gas leaving the reactor is: $C_{out}^{inert} = 100 - C_{out}^{CO_2} - C_{out}^{O_2}$.

- Since yeast do not consume or produce nitrogen and argon, the change (if any) in the concentrations of these inert gases between the air entering the reactor (C_{in}^{inert}) and the gas leaving the reactor (C_{out}^{inert}) must be due to a change in the volume of gas leaving the reactor per unit time. Mass conservation requires that $C_{in}^{inert} J_{in} \equiv C_{out}^{inert} J_{out}$, and thus we compute flux of

gas leaving the reactor as:

$$J_{out}(t) = J_{in}\frac{C_{in}^{inert}}{C_{out}^{inert}(t)} = J_{in}\frac{100 - C_{in}^{CO_2} - C_{in}^{O_2}}{100 - C_{out}^{CO_2}(t) - C_{out}^{O_2}(t)} \tag{1}$$

In our experiments J_{in} is generally large relative to the gases consumed and produced by our cultures, resulting in small changes in the concentrations of carbon dioxide and oxygen, and thus J_{out} differs only slightly from J_{in}.

Accounting for Buffering

The application of mass conservation to our data allows us to compute the fluxes of oxygen and carbon dioxide, Ψ_{O_2} and Ψ_{CO_2} respectively, based on equations (2-3). To convert these fluxes into units of moles per hour (mol/h), we divide them by the molar volume (V_m) of air at the lab temperature (25^oC) and pressure (1 atmosphere), ($V_m = 24.47\ dm^3/mol$).

$$\Psi_{O_2} = \frac{1}{V_m}\left[J_{in}C_{in}^{O_2} - J_{out}C_{out}^{O_2}\right] \tag{2}$$

$$\Psi_{CO_2} = \frac{1}{V_m}\left[J_{in}C_{in}^{CO_2} - J_{out}C_{out}^{CO_2}\right] \tag{3}$$

The Ψ fluxes are primarily due to the gases consumed and produced by the cells. However, Ψ are also affected, to a much smaller extent, by the buffering reaction of the growth medium and the air present in the reactor and the tubing system carrying the exhaust gas to the detectors. Since we have precise measurements for the physical characteristics of our system, we can compute the contribution of the buffering according to equations (4-5) and subtract it, if necessary, to obtain a better estimate of fluxes due only to cellular metabolism.

$$\text{Buffering}^{O_2} = \frac{\partial C_{out}^{O_2}}{\partial t}\left[\underbrace{k_H^{O_2} V_{\text{medium}}}_{\text{Medium}} + \underbrace{\frac{1}{V_m} V_{\text{Air}}}_{\text{Air}}\right] \tag{4}$$

$$\text{Buffering}^{CO_2} = \frac{\partial C_{out}^{CO_2}}{\partial t}\left[\underbrace{k_H^{CO_2} V_{\text{medium}}}_{\text{Medium}} + \underbrace{\frac{1}{V_m} V_{\text{Air}}}_{\text{Air}}\right] \tag{5}$$

Where $k_H^{O_2}$ and $k_H^{CO_2}$ are the Henry's constants at 1 atmosphere pressure for oxygen and carbon dioxide respectively, with values $k_H^{O_2} = 1.3 \times 10^{-3}\ mol/L$ and $k_H^{CO_2} = 3.4 \times 10^{-2}\ mol/L$. V_{Medium} and V_{Air} are the volume of the culture (growth medium) and the volume of the air in the reactor and the tubing system. In the conditions of our experiments, the contribution of the buffering is quite small relative to the fluxes due to cellular metabolism. The terms due to the air in the reactor and the tubing are small because the volume of air is small relative to the volume of the culture; typically, the volume of air in the system is an order of magnitude smaller than the culture volume. The term due to dissolved oxygen is also very small because oxygen has low solubility in water $k_H^{O_2}$. The largest buffering term is due to the dissolved carbon dioxide and even it is quite small relative to the total flux due to cellular metabolism. When the changes in the concentrations of carbon dioxide and oxygen are small relative to J_{in}, their time derivatives are small too, and thus equations (4-5) indicate that the contribution of the buffering is going to be rather small too.

Empirical Validation of Measured O_2 and CO_2 Fluxes

We used a series of control experiments to test the estimates based on the above steps. These experiments used the same growth media as the media used for the experiments and included switching the incoming gas aerating the reactor from air to medical atmosphere (air containing $5\%\ CO_2$) or nitrogen and back. For each switch, we collected data continuously and used them to test and validate the buffering estimates based on equations (4-5). Importantly, none of the results

in the main paper depend on the small corrections for buffering.

Measuring oxygen consumption at low biomass density is exceedingly challenging since the cells consume a very small fraction of the oxygen passing through the reactor and even relatively small errors in the oxygen concentration can have a large impact on the estimated oxygen consumption. To evaluate whether our experimental setup can estimate oxygen consumption in such regime of low biomass, we conducted control experiments.

The first control experiment designed specifically to address the accuracy of flux measurements at low biomass densities was identical to the experiment described in the paper except for the carbon source: instead of 11.11 mM glucose, the media contained 100 mM ethanol as a sole source of carbon and energy (Slavov and Botstein, 2011). The complete oxidation of an ethanol molecule requires 3 O_2 molecules and produces 2 CO_2 molecules. Thus, chemical stoichiometry and mass-conservation require that the respiratory quotient (RQ, defined as the molar ratio of produced CO_2 and consumed O_2) for ethanol oxidation equals 2/3, providing a strong benchmark for evaluating the accuracy of our measurements in conditions as close as possible to these used for the experiments described in the paper. Of course, cells growing on ethanol as a sole source of carbon and energy can either have a new synthesis or degradation of reserved carbohydrates (trehalose and glycogen) which would result in small deviation of the RQ from the 2/3 expected for oxidizing ethanol. The results of this experiment (Figure 1B) indicate that the experimentally measured RQ equals the expected RQ (2/3) both at low biomass density (lower than in Figure 2) and across over 7 doubling periods corresponding to over 2 orders of magnitude in the dynamical ranges of the measured gases. Thus, increase of O_2 consumption and CO_2 production does not bias our experimental estimates of these fluxes and the respiratory quotient.

The second control experiment was designed specifically to address the accuracy of flux measurements at low biomass densities with glucose as the sole carbon source to better control for our main experiments. The experiment was identical to the experiment described in the paper except for a 40 fold lower concentration of the carbon source: instead of 2g/L (11.11 mM) glucose, the media contained 50mg/L (278 mM) glucose as a sole source of carbon and energy. With this exper-

iment we aimed to further evaluate the accuracy of our flux measurements at even lower biomass and in media having the same carbon source (glucose) as the one used in our experiments. We took advantage of the well established observation that when budding yeast is grown at very low glucose levels for long periods of time, it mostly oxidizes glucose to CO_2 and H_2O and only a very small fraction of the glucose is fermented to ethanol (Küenzi and Fiechter, 1969; Hoek et al., 1998; van Hoek P et al., 2000). The results of this experiment (Figure S1) indicate that the experimentally measured RQ remains constant over several doubling times and equals the expected RQ (1.2) for the experimental levels of glucose and growth rate (Küenzi and Fiechter, 1969; Hoek et al., 1998; van Hoek P et al., 2000).

These control experiments establish that our experimental system is able to measure the expected RQ values at low biomass densities. Furthermore, the estimated RQ values remain constant over many doubling times and several orders of magnitude change in biomass density and O_2 and CO_2 fluxes. Therefore, we conclude that while low biomass density presents a formidable challenge to measuring metabolic fluxes and RQ, our experimental design has overcome these challenges; the increase in RQ in Figure 3 is unlikely to be an artifact of the low biomass density or simply the increase of the measured fluxes of O_2 and CO_2.

Controlling for Oxygen Limitation

Oxygen limitation in the course of our experiments is an important factor to control for. We measured dissolved oxygen in the media with a Clark electrode and the dissolved oxygen always followed the oxygen levels in the exhaust gas, remaining above 80 % oxygen saturation at all times and above 90 % oxygen saturation during the first exponential phase when oxygen consumption per cell decreases. Furthermore, we performed independent experiments with different levels of aeration (varying over 8 fold dynamical range) and computed the same fluxes of oxygen, further corroborating that oxygen limitation was not a factor influencing our results.

Estimating ATP Flux

The total rate of ATP production (Ψ_{ATP}) can be estimated as a sum of the ATP produced by oxidative phosphorylation in the mitochondria and the ATP produced by fermenting glucose to ethanol. The rate of ATP produced by oxidative phosphorylation equals the flux of oxygen consumption times the number of ATP molecules generated per oxygen atom consumed, known as P/O ratio. Since the P/O ratio is hard to measure *in vivo*, multiple P/O ratios have been reported (Sheldon et al., 1996; Campbell et al., 1985; Hinkle, 2005). We used values (low limit $P/O = 1$ and high limit $P/O = 2.2$) encompassing the reported range. In addition, each completely oxidized molecule of glucose generates 2 ATPs from glycolysis and 2 GTPs, which are the equivalent of 2 ATPs, from substrate level phosphorylation during the tricarboxylic acid cycle. The rate of ATP produced by fermentation equals the flux of ethanol production, which is equivalent to the flux of CO_2 minus the flux of O_2, times 1 molecule of ATP produced by substrate level phosphorylation in the process. Thus, the total ATP flux (Ψ_{ATP}) was estimated from the fluxes of carbon dioxide (Ψ_{CO_2}) and oxygen (Ψ_{O_2}) according to: $\Psi_{ATP} = (P/O + 1/3) \times 2 \times \Psi_{O_2} + 1 \times (\Psi_{CO_2} - \Psi F_{O_2})$.

The above estimate accounts for the two main sources of ATP, glycolysis and oxidative phosphorylation, whose absolute rates we have measured directly and used for computing the ATP flux. In addition, small amounts of ATP could be released by biosynthetic reactions. Since the rate of biosynthesis is constant during the period of exponential growth considered in our analysis, these small sources can contribute at most a small constant term, which cannot account for the trend in the ATP flux that we observed (Figure 3). The conclusion that the ATP flux decrease does not depend on the exact values that we use for the efficiency of fermentation and oxidative phosphorylation: since since O_2 consumption per cell decreases (Figure 2F) and CO_2 production per cell remains steady or decreases slightly (Figure 2G), any positive efficiencies of fermentation and respiration will result in a declining ATP flux.

Mass Balance of Carbon

We sought to cross-check our measurements of metabolic fluxes (O_2, CO_2, and glucose) and of cell biomass by evaluating, at each time point of the first phase of exponential growth, whether the uptake of carbon equals its secretion and incorporation into biomass. This analysis allows using mass-conservation to evaluate the error in the data. The flux of consumed carbon (F^C_{in}) should equal the total flux of secreted carbon (F^C_{out}). Since glucose is the sole carbon source in our experiments F^C_{in} equals the flux of carbon intake from glucose (equation 6). F^C_{out} can be estimated from its major components, the fluxes of respiration ($F^C_{respiration}$), fermentation ($F^C_{fermentation}$), and biomass incorporation ($F^C_{biomass}$) according to equation 7. The estimation of these fluxes and their balance is described in the subsections below and shown in Figure 3.

$$F^C_{in} = F^C_{glucose} \tag{6}$$

$$F^C_{out} = F^C_{respiration} + F^C_{fermentation} + F^C_{biomass} \tag{7}$$

All fluxes ($F^C_{process}$) represent millimoles (mmol) of carbon per hour from the subscripted process.

Flux of Glucose and Carbon Consumption

To estimate the glucose consumption, we measured the residual glucose concentration in triplicate (using R-biopharm enzymatic kit) in the growth medium in the course of our experiment (Figure S3). The derivative of this measured time-series data equals the rate (flux) of glucose consumption. Since glucose is the sole source of carbon in our medium and each molecule of glucose has 6 carbon atoms, the flux of carbon consumption ($F^C_{glucose}$) equals 6 times the flux of glucose consumption.

Flux of Carbon Secretion and Biomass Incorporation

Since the oxidation of a glucose molecule requires 6 molecules of O_2 and produces 6 molecules of CO_2, the respiratory flux ($F^C_{respiration}$) equals the flux of oxygen consumption (Figure 2). The flux of carbon released via fermentation ($F^C_{fermentation}$) can be estimated both from the measured ethanol concentrations (Figure S3) as 3/2 the carbon released with the ethanol flux or as 3 times the flux of CO_2 due to fermentation, which is the total CO_2 flux minus the O_2 flux. We use the latter because of the much higher accuracy of the gas measurements, because of its greater reliance and thus check of the oxygen flux, and because of potential complications from the volatility of ethanol; the two estimates agree closely. Finally, the flux of carbon incorporated into biomass ($F^C_{biomass}$) can be estimated from the ratio of gDW over the atomic molar mass of carbon (12), times the growth rate (μ), times the carbon content of dry yeast biomass, which is measured to be $48\ \%$ (Verduyn et al., 1991; Hoek et al., 1998). Thus, $F^C_{biomass} = 0.48\frac{gDW}{12}\mu$.

The fluxes of carbon consumption (F^C_{in}) equal the fluxes of carbon secretion and biomass incorporation (F^C_{out}) computed from the data (Figure 3B), suggesting that our measurements are mutually consistent and can account for the fluxes in our experiments.

Measuring Stress Resistance

Stress resistance was measured as described previously(Slavov et al., 2012). Briefly, from each quantified time point, a sterile sample of $1\ ml$ culture was taken and split into three tubes, each containing $250\ \mu l$. The first tube (control) was kept at 30^oC and the remaining two tubes, each tube corresponding to either heat-shock or oxidative-shock, were either dropped in water bath at 48^oC or mixed with H_2O_2 to a final H_2O_2 concentration of $5\ mM$. After $10\ min$, the samples subjected to heat and H_2O_2 were removed and all samples washed several times with liquid YPD (YPD; 10 g of Bacto-Yeast extract, 20 g of Bacto-peptone, and 20 g of glucose in 1000 ml of water).

Each sample was serially diluted $1:10$ with liquid YPD into 9 dilutions spanning 9 orders of magnitude. The dilutions were spread on YPD (YPD; 10 g of Bacto-Yeast extract, 20 g of Bacto-

peptone, 20 g of Bacto-agar, and 20 g of glucose in 1000 ml of water) plates to measure viability. Colonies were counted after $36\ h$ incubation at $30\ ^oC$. For each time point, a minimum of 100 colonies were counted. The fraction of viable cells in a sample was quantified as the fraction of cells surviving the heat or the H_2O_2 exposure relative to the corresponding control, the cells that were not exposed to stress.

The colony forming units from the controlled samples are in excellent agreement with the cell densities measured by the Coulter counter, indicating that the cells in our cultures had higher than $99\ \%$ viability and that the procedure used to measure stress resistance did not result in loss of cells.

Measuring Messenger RNA Levels

The cells were harvested by vacuum filtering the samples followed by immediately freezing the cells in liquid nitrogen and then in a freezer at -80^oC. RNA for microarray analysis was extracted by the acid–phenol–chloroform method. RNA was amplified and labeled using the Agilent low RNA input fluorescent linear amplification kit (P/N 5184-3523; Agilent Technologies, Palo Alto, CA). This method involves initial synthesis of cDNA by using a poly(T) primer attached to a T7 promoter. Labeled cRNA is subsequently synthesized using T7 RNA polymerase and either *Cy3* or *Cy5* UTP. Each *Cy5*-labeled experimental cRNA sample was mixed with the *Cy3*-labeled reference cRNA and hybridized for 17 h at 60^oC to custom Agilent Yeast oligo microarrays $8 \times 44k$ having 8 microarrays per glass slide. Microarrays were washed, scanned with an Agilent DNA microarray scanner (Agilent Technologies), and the resulting TIF files processed using Agilent Feature Extraction Software version.

Measuring Protein Levels and Post-translational Modifications

For each time point we harvested at least 10^8 cells by $90\ sec$ centrifugation at $3,000 \times g$, followed by immediate freezing of the cells in liquid nitrogen and then in a freezer at -80^oC.

Extracting total protein

We used insoluble protein buffer (IPB) at pH 8.5 with the following composition: 50 mM Tris-HCl, 150 mM NaCl, 8 M urea, 2 % SDS, 1mM PMSF, 2mM DTT, 1:1000 Pierce protease inhibitors. The IPB was made fresh just before each use.

The cell pellet from each time-sample was suspended with $50\ \mu l$ IPB and pipeted over a metal ball cooled to a liquid nitrogen temperature in a 2 ml tube. The tubes were positioned into the PTFE 2mL tube adapter for the Retsch Mixer Mill MM400 (Retsch 22.008.0005) and the entire assembly submerged into liquid nitrogen. After the bubbling of the liquid nitrogen stopped, the assembly was mounted on the Retsch Mixer Mill MM400 and agitated for 90 seconds at 30 Hz.

The agitation was repeated 4 to 6 times and between the agitations the sample holder was returned to liquid nitrogen for cooling. Complete lysis produced fine snowy powder in the tube.

After pulverizing the cells into fine powder, the protein was dissolved by adding $450\ \mu l$ IPB and the metal ball used to pulverize the cells extracted with a magnet. The resulting $500\ \mu l$ suspension was moved to a fresh tube, span at $20,000 \times g$ for 5 minutes and the supernatant (the total protein fraction) separated for further purification by the chloroform-methanol method described below.

Chloroform–methanol Purification of Proteins

To $500 \mu l$ protein sample (about $500 \mu g$ protein) in a 15 ml falcon tube:

1. Add 2ml methanol and vortex thoroughly.
2. Add $500\ \mu l$ chloroform and vortex.
3. Add $1500\ \mu l$ water and vortex; the mixture become cloudy with precipitated protein flakes.
4. Centrifugation for 1 minute at $14,000 \times g$ resulted is three layers: a large aqueous layer on top, a circular flake of protein in the interphase, and a smaller chloroform layer at the bottom.
5. Remove top aqueous layer carefully, trying not to disturb the protein flake.
6. Add $2ml$ methanol and vortex.
7. The resulting mixture was centrifugated for 5 minutes at $20,000 \times g$, which pelleted the purified protein.
8. We removed as much methanol as possible with care since the pellet is delicate.
9. The protein pellet was dried under vacuum.

Sample Preparation

A 100 μg of total protein from each time-point-sample were digested using slightly modified FASP protocol (Wiśniewski et al., 2009). Subsequently each time-point-sample was labeled with TMT-6plex reagent (Prod # 90061, Thermo Fisher, San Jose, CA) according to a manufacturer protocol. Each set of 6 time-point-sample, labeled with the 6 distinct TMT mass tags, were pooled into one set-sample. This sample was fractionated by electrostatic repulsion-hydrophilic interaction

chromatography chromatography (ERLIC) run on an HPLC 1200 Agilent system using PolyWAX LP column (200x2.1 mm, 5 μm, 30nm, PolyLC Inc, Columbia, MD) and with a fraction collector (Agilent Technologies, Santa Clara, CA). Set-samples were fractionated into a total of 25 fractions on a $70\ min$ liquid chromatography (LC) gradient. Each ERLIC fraction was subsequently further separated by HPLC and submitted for tandem mass spectrometry analysis.

Tandem Mass Tags (TMT) Mass–spectrometry

All fractions were run on Orbitrap Velos Pro (Thermo Fisher, San Jose, CA). HPLC fractions were injected from auto-sampler into the trapping column and then eluted on capillary column ($75\ \mu m$ inner diameter $\times$ 5 cm length, packed with $5\ \mu m$ beads from Michrom Bioresources, Inc.). The fractions were eluted with a $90\ min$ gradient of acetonitrile $2 - 32\ \%$ in $0.1\ \%$ formic acid. The instrument was set to run in TOP 10 MS/MS mode method with dynamic exclusion. After MS1 scan in Orbitrap with 30K resolving power, each ion was submitted to an HCD MS/MS with 7500 resolving power and to CID MS/MS scan subsequently. All quantification data were derived from HCD spectra.

B (30

Analysis of MS Spectra

Mass/charge spectra where analyzed by MaxQuant (version 1.3.0.5) (Cox and Mann, 2008), Proteome Discover (Beta version 1.4.0.282, Thermo), Mascot (2.4, Matrix Science). Searches were performed against an yeast proteome database and common contaminants that were added to this database. Searches had trypsin enzyme specificity, allowing 2 missed cleavages. Variable modifications included in the search parameters were Met oxidation, Asn deamidation, Lys and Arg acetylation and Ser, Thr and Tyr phosphorylation. The search criteria were held at $1\ \%$ FDR on both protein and on peptide levels and $2\ \%$ for peptides with posttranslational modifications.

Measuring Cytoplasmic Amino Acid Concentrations

Analysis of underivatized amino acids was performed by liquid-chromatography tandem mass-spectrometry (LC/MS/MS) on an Agilent (Agilent Technologies, Santa Clara, CA) 6460 triple-

quadrupole LC/MS/MS system. Ions were monitored via electrospray ionization in the positive ion mode with multiple reaction monitoring (MRM). LC separations were carried out with a Phenomenex (Torrance, CA) Luna 5u SCX strong cation exchange column. For elution of the amino acids 30 mM ammonium acetate in water (solvent A) and 5% acetic acid in water (solvent B) were applied in two consecutive isocratic elution steps. An external standard curve mixture was analyzed at various concentrations $2\mu M - 200\mu M$ and used for absolute quantification. Note that we cannot distinguish Leu and Ile from their mass/charge spectra.

Analysis of Gene Regulation

The most basic question to ask from the measured mRNA and protein levels is which mRNAs and proteins change significantly (in a formal statistical sense) during the phases of exponential growth. The significance of such differences may be estimated for each time point based on the concordance of the measured levels of different peptides corresponding to the same protein (we measure on average a dozen peptides per protein) or from the null distributions estimated from biological replicas. We focused on monotonic trends in time (increasing or decreasing levels of mRNAs/proteins as a function of time) during each of the two phases of exponential growth. Such monotonic trends were quantified by two independent approaches: (i) Spearman rank correlation between the time of measuring the levels of mRNA/protein and the measured levels, resulting in correlations quantifying the trends of change and (ii) linear regression of the time of measuring the levels of mRNA/protein on the measured levels, resulting in slopes quantifying the trends of change. As a measure of goodness of fit of the linear models, we use the fraction of variance explained by the model, which for the j^{th} mRNA/protein is quantified by R_j^2:

$$R_j^2 = 1 - \frac{\sum_{i\in\alpha}(y_{ij} - f_{ij})^2}{\sum_{i\in\alpha}(y_{ij} - \bar{\mathbf{y}}_j)^2} \tag{8}$$

In (8), $\mathbf{y}_j$ is a vector of levels of the j^{th} mRNA/protein (j^{th} column in $\mathbf{Y}$), $\bar{\mathbf{y}}_j$ is its mean expression level, i is index enumerating the set of time points α used in the model and f_{ij} is the model predication for the i^{th} time point and j^{th} mRNA/protein.

For both metrics (correlations and slopes), we computed null distributions based on $20,000$ random permutations of the data. From the null distributions, we computed the probability of

observing the observed changes by chance alone (p values) and converted the p values into q values estimating the false discovery rate (FDR) to correct for multiple hypothesis testing.

Once we defined sets of genes based on the changes of their mRNAs and protein levels, we sought to identify whether some biological functions are over-represented within a set. Such analysis can be done by the widely–used gene ontology (GO) term finder (GO Term Finder (Boyle et al., 2004)). The results indicated very statistically significant enrichment for a large number of biological functions. During the first phase (Figure 4A), genes decreasing both at the mRNA and protein levels are highly ($p < 10^{-42}$) enriched for ncRNAs metabolic process, ribosome biogenesis, rRNA processing, amino acids and tRNAs processing; genes increasing at the mRNA and protein levels are enriched ($p < 10^{-20}$) for oxidation-reduction process, generation of metabolites and energy, glycogen & trehalose metabolism. During the second phase (Figure 4B), genes decreasing both at the mRNA and protein levels are highly ($p < 10^{-33}$) enriched for mitochondrial translation and organization, biosynthesis, translation, amino acids, ncRNA, rRNA; genes increasing at the mRNA and protein levels are enriched ($p < 10^{-14}$) for catabolism, oxidation-reduction process, carbohydrate metabolism, gluconeogenesis, glycolysis, and generation of metabolites and energy.

While the GO terms finder is a useful tool for identifying functional groups of genes, it has a number of drawbacks including hard thresholding, data discretization (binarization and the associated loss of information), and decreased statistical power for GO terms with a small number of genes (Slavov and Botstein, 2010). To overcome these drawbacks, we applied non–parametric statistical analysis for identifying sets of genes with statistically significant responses. This analysis makes use of prior knowledge of biological networks and metabolic pathways (or even the GO terms) to identify sets of genes. For each set, the distribution of responses (such slopes computed from regressing the mRNA/protein levels on time) of the genes that belong to the set is compared to the distribution of responses to all genes. The statistical significance of the difference between the two distributions, if any, is computed from the nonparametric Wilcoxon rank–sum (Mann Whitney) test. It is a non-parametric test for comparing two distributions without making assumptions about their shapes and gives the probability of obtaining greater observations in one population versus the other by chance alone. The null hypothesis in the rank–sum test is that both samples have the same probability of exceeding each other. We used this approach to systematically evaluate the all biochemical pathways curated by the *Saccharomyces* Genome Database (SGD). All p values were corrected for multiple hypotheses testing by converting them into q values quantifying

the false discovery rate (FDR).

Decline in Folate-mediated Mitochondrial NADPH Production and One-carbon Metabolism

The biochemical pathways with significant dynamics during phase 1 show very strong enrichment (consistent decline at both mRNA and protein level, FDR $\ll 1\%$) for folate metabolism, involved in one-carbon (methyl) transfer, and the serine hydroxymethyltransferases, generating methyl groups from the conversion of serine to glycine (Figure S4 and Figure 4). The intracellular concentrations of both serine and glycine remain constant throughout phase 1 (albeit they plummet after the di-auxie shift; Figure S5B) suggesting that the decline in serine hydroxymethyltransferases is related to the decline in producing methyl groups; this suggestion is further supported by a parallel decline in serine biosynthesis from 3-phosphoglycerate. Thus, the levels of all enzymes (and their corresponding mRNAs) catalyzing reactions mitochondrial NADPH from from 3-phosphoglycerate decline during the first phase of constant doubling time.

Inferring TF Regulation

One of simplest approaches to identifying transcription factors (TF) that might contribute to the measured transcriptional response is to compute the overlap between a set of genes with similar expression profiles, such as increasing or decreasing during the phase of constant growth rate (Figure S2 and Figure 4), and the targets of a TF as identified independently from chromatin immunoprecipitation experiments (Harbison et al., 2004; MacIsaac et al., 2006). Given a set of n genes selected based on their increase or decrease during exponential growth out of all $N = 6000$ genes and a TF regulating T target genes, the probability of observing an overlap of k genes between the two gene sets by chance alone (*p value*) is given by the cumulative mass function of the hypergeometric distribution, eq. 9:

$$P(X \geq k|N,T,n) = \sum_{i=k}^{i=T} \frac{\binom{T}{i}\binom{N-T}{n-i}}{\binom{N}{n}} = 1 - \sum_{i=0}^{i=k-1} \frac{\binom{T}{i}\binom{N-T}{n-i}}{\binom{N}{n}} \tag{9}$$

The p-values in Table 1 are computed based on the TF targets published by MacIsaac et al. (2006) at $p \leq 0.001$ and conservation level 1. Chief advantages of this approach are its simplic-

ity and the avoidance of assumptions, such as approximating TF activities with the levels of the corresponding mRNAs. This approach lacks power to identify all TFs because of the incomplete knowledge of the transcriptional network. Nonetheless, the rate of false positives is very low: A low *p value* for the overlap of the targets of the i^{th} TF and the j^{th} gene set indicates high probability that the i^{th} TF regulates the j^{th} gene set. Characterizing combinatorial regulation (Slavov and Dawson, 2009; Petti et al., 2011) and building quantitative models requires more advanced analysis, such as network inference algorithms (Markowetz and Spang, 2007; Slavov, 2010) and further experimental testing.

References

Boyle, E. I., Weng, S., Gollub, J., Jin, H., Botstein, D., Cherry, J. M. and Sherlock, G. (2004). GO::TermFinder–open source software for accessing Gene Ontology information and finding significantly enriched Gene Ontology terms associated with a list of genes. Bioinformatics (Oxford, England) *20*, 3710–3715.

Brauer, M. J., Saldanha, A. J., Dolinski, K. and Botstein, D. (2005). Homeostatic Adjustment and Metabolic Remodeling in Glucose-limited Yeast Cultures. Molecular Biology of the Cell *16*, 2503–2517.

Bryan, A., Engler, A., Gulati, A. and Manalis, S. (2012). Continuous and long-term volume measurements with a commercial coulter counter. PloS one *7*, e29866.

Campbell, S., Jones, K. and Shulman, R. (1985). In vivo ^{31}P nuclear magnetic resonance saturation transfer measurements of phosphate exchange reactions in the yeast *Saccharomyces cerevisiae*. FEBS letters *193*, 189–193.

Cox, J. and Mann, M. (2008). MaxQuant enables high peptide identification rates, individualized ppb-range mass accuracies and proteome-wide protein quantification. Nature biotechnology *26*, 1367–1372.

Harbison, C. T., Gordon, D. B., Lee, T. I., Rinaldi, N. J., Macisaac, K. D., Danford, T. W., Hannett, N. M., Tagne, J., Reynolds, D. B., Yoo, J., Jennings, E. G., Zeitlinger, J., Pokholok, D. K., Kellis,

M., Rolfe, P. A., Takusagawa, K. T., Lander, E. S., Gifford, D. K., Fraenkel, E. and Young, R. A. (2004). Transcriptional regulatory code of a eukaryotic genome. Nature *431*, 99–104.

Hickman, M. and Winston, F. (2007). Heme levels switch the function of Hap1 of Saccharomyces cerevisiae between transcriptional activator and transcriptional repressor. Molecular and cellular biology *27*, 7414–7424.

Hinkle, P. (2005). P/O ratios of mitochondrial oxidative phosphorylation. Biochimica et Biophysica Acta (BBA)-Bioenergetics *1706*, 1–11.

Hoek, P. V., Dijken, J. P. V. and Pronk, J. T. (1998). Effect of Specific Growth Rate on Fermentative Capacity of Baker's Yeast. Applied and Environmental Microbiology *64*, 4226–4233.

Küenzi, M. T. and Fiechter, A. (1969). Changes in carbohydrate composition and trehalase-activity during the budding cycle of Saccharomyces cerevisiae. Archiv Fr Mikrobiologie *64*, 396–407.

MacIsaac, K. D., Wang, T., Gordon, D. B., Gifford, D. K., Stormo, G. D. and Fraenkel, E. (2006). An improved map of conserved regulatory sites for Saccharomyces cerevisiae. BMC Bioinformatics *7*, 113–113.

Markowetz, F. and Spang, R. (2007). Inferring cellular networks–a review. BMC bioinformatics *8*, S5.

Petti, A. A., Crutchfield, C. A., Rabinowitz, J. D. and Botstein, D. (2011). Survival of starving yeast is correlated with oxidative stress response and nonrespiratory mitochondrial function. Proceedings of the National Academy of Sciences *108*, E1089 E1098.

Sheldon, J., Williams, S., Fulton, A. and Brindle, K. (1996). ^{31}P NMR magnetization transfer study of the control of ATP turnover in *Saccharomyces cerevisiae*. Proceedings of the National Academy of Sciences *93*, 6399.

Slavov, N. (2010). Inference of Sparse Networks with Unobserved Variables. Application to Gene Regulatory Networks. JMLR W&CP *9*, 757–764.

Slavov, N., Airoldi, E. M., van Oudenaarden, A. and Botstein, D. (2012). A conserved cell growth cycle can account for the environmental stress responses of divergent eukaryotes. Molecular Biology of the Cell *23*, 1986–1997.

Slavov, N. and Botstein, D. (2010). Universality, specificity and regulation of S. cerevisiae growth rate response in different carbon sources and nutrient limitations. PhD thesis, Princeton University.

Slavov, N. and Botstein, D. (2011). Coupling among growth rate response, metabolic cycle, and cell division cycle in yeast. Molecular Biology of the Cell *22*, 1997–2009.

Slavov, N. and Dawson, K. A. (2009). Correlation signature of the macroscopic states of the gene regulatory network in cancer. Proceedings of the National Academy of Sciences *106*, 4079–4084.

Slavov, N., Macinskas, J., Caudy, A. and Botstein, D. (2011). Metabolic cycling without cell division cycling in respiring yeast. Proceedings of the National Academy of Sciences of the United States of America *108*, 19090–19095.

van Hoek P, van Dijken JP and Pronk (2000). Regulation of fermentative capacity and levels of glycolytic enzymes in chemostat cultures of Saccharomyces cerevisiae. Enzyme and Microbial Technology *26*, 724–736.

Verduyn, C., Stouthamer, A., Scheffers, W. and Dijken, J. (1991). A theoretical evaluation of growth yields of yeasts. Antonie van Leeuwenhoek *59*, 49–63.

Wiśniewski, J., Zougman, A., Nagaraj, N. and Mann, M. (2009). Universal sample preparation method for proteome analysis. Nature methods *6*, 359–362.

Zampar, G. G., Kümmel, A., Ewald, J., Jol, S., Niebel, B., Picotti, P., Aebersold, R., Sauer, U., Zamboni, N. and Heinemann, M. (2013). Temporal system-level organization of the switch from glycolytic to gluconeogenic operation in yeast. Molecular systems biology *9*, 651.

Supplemental Figures and Captions

Figure S1. Rates of O_2 Consumption and CO_2 Production during Batch Growth in Media Containing $50\ mg/L$ Glucose as a Sole Source of Carbon and Energy
(A) Cell density (single cells per ml) during exponential growth on glucose.
(B) The levels of O_2 in the exhaust gas were measured continuously (every second) with ZrO_2 cell.
(C) The levels of CO_2 in the exhaust gas were measured continuously (every second) with infra red spectroscopy.
(D) Fluxes of O_2 uptake Ψ_{O_2} and CO_2 production Ψ_{CO_2} estimated from the data in (A) and (B) and eqn. 1-5.
(E) Respiratory quotient (RQ), defined as the ratio of Ψ_{CO_2} to Ψ_{O_2}.
Related to Figure 1.

Figure S2. The Growth Rate and the Doubling Period of Batch Cultures Remains Constant for 9 Generations.
(A) Yeast batch cultures growing in minimal medium were sampled every $10 - 15\ min$ and at each time-point optical density at $600\ nm$
(B) Number of cell per ml of culture.
(C) Cell size distributions plotted as a heat map indicating the percent of cells in each bin.
Related to Figure 2.

Figure S3. Concentrations of Residual Glucose and Generated ethanol in the Growth Medium. Concentrations were measured with the enzymatic R-Biopharm kits.
Related to Figure 3.

Figure S4. Global Remodeling of mRNA and Protein Regulation during Batch Growth at a Constant Growth Rate.
(A) The same time-point protein sample was labeled with different TMT tags (127 or 130) the labeled fractions mixed at $1/0.6$ ratio; The ratio in the figure is estimated empirically by regression and the correlation coefficient is computed based on all quantified peptides, $5\ 237$ in total. The color-code reflects the density of datapoints.
(B) Levels of human proteins from the dynamic universal proteomics standard (USP2). UPS2 was spiked at different levels (x-axis) in the total yeast protein extract and quantified by TMT. The levels quantified by TMT (y-axix) correspond closely to the spiked levels. The lowest spiked amount in the first channel is set to 1 for all proteins and all other levels reported as fold increase relative to the first TMT channel.
(C) Metabolic pathways and biological functions that change significantly during growth at a constant doubling time. During the phases of constant doubling periods, the dynamics of genes within a pathway, quantified by regression slopes, were compared to the time dynamics for all genes. The gene ontology (GO) terms that show significant dynamics (FDR $< 1\%$). The magnitude of change for each gene set is quantified as the average percent change in the level of its genes per doubling period of the cells.
(D) The same as in C but for biochemical pathways at FDR $< 2\%$.
Related to Figure 4.

Figure S5. Transcriptional, Metabolic and Post-translational Dynamics during Batch Growth at a Constant Rate
(A) The levels of all enzymes (and their corresponding mRNAs) catalyzing reactions of the tricarboxylic acid (TCA) cycle. Many mRNAs increase in abundance gradually but the levels of the corresponding enzymes (proteins) do not change until the very last time point, just before the growth stops. The enzymes encoded by mRNAs whose levels decease also decrease in concert with the mRNAs. The data are displayed on a $\log_2$ scale with 2 fold dynamical range.
(B) The mRNAs of hydroperoxide and superoxide-radicals induced glutathione-dependent oxidoreductases (RGX) decline during growth at a constant doubling time. The hydroperoxide and superoxide-radicals induced mRNAs coding for GRX3 and GRX4 decrease, parallel to the decreased oxygen consumption (Figure 2F), during the first exponential growth phase. Data are displayed on a $\log_2$ scale.
(C) Intracellular amino acid levels during the diauxic shift. The levels of intracellular amino acid were measured my liquid chromatography tandem mass-spectrometry (LC-MS/MS) are displayed on a $\log_2$ scale.
(D) Dynamic Changes of Acetylated Peptides during Batch Growth at a Constant Rate. The levels of hundreds of acetylated peptides, measured my liquid chromatography tandem mass-spectrometry (LC-MS/MS), are displayed on a $\log_2$ scale. The peptides are arranges based on their rate of change relative to time as computed by a linear regression. Related to Figure 5.

Figure S1

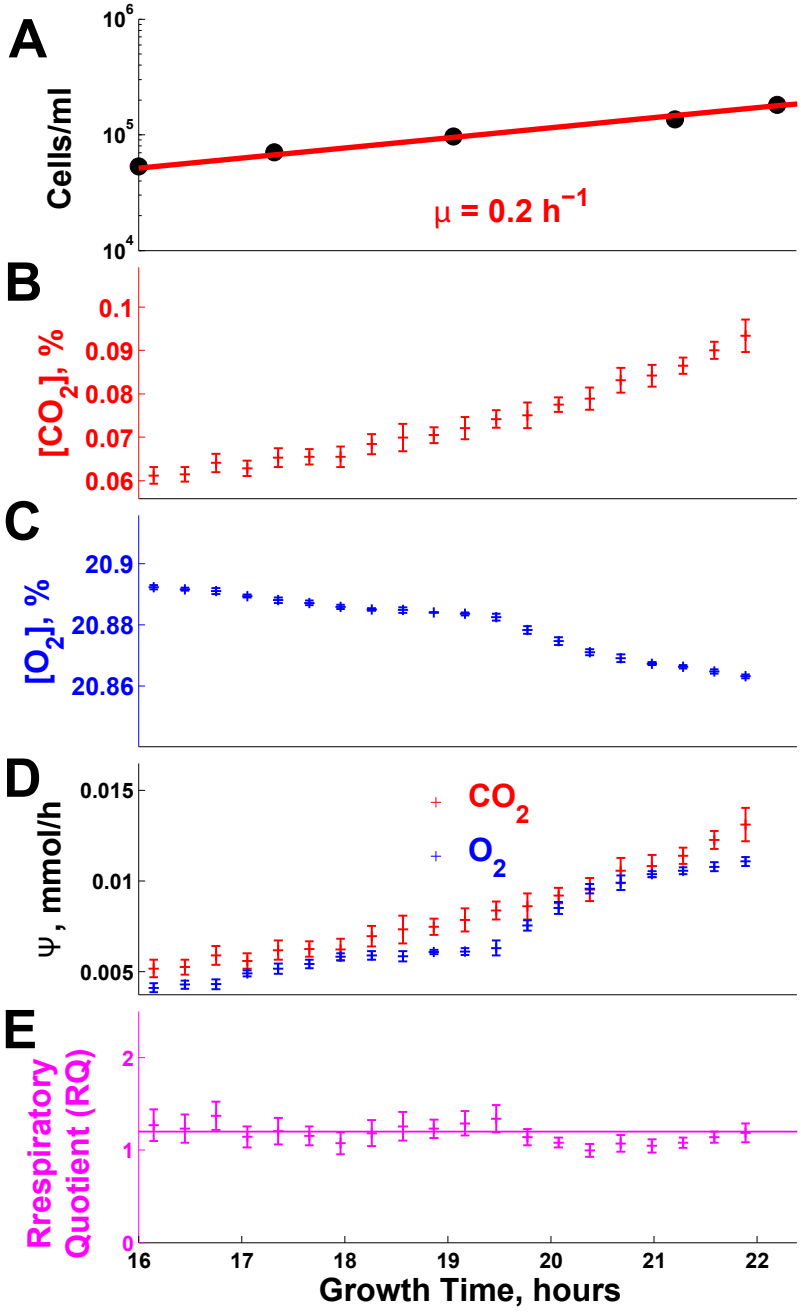
A
Cells/ml
10^6
10^5
10^4
μ = 0.2 h^{-1}
B
$[CO_2]$, %
0.1
0.09
0.08
0.07
0.06
C
$[O_2]$, %
20.9
20.88
20.86
D
Ψ, mmol/h
0.015
0.01
0.005
CO_2
O_2
E
Rrespiratory Quotient (RQ)
2
1
0
16
17
18
19
20
21
22
Growth Time, hours

Figure S2

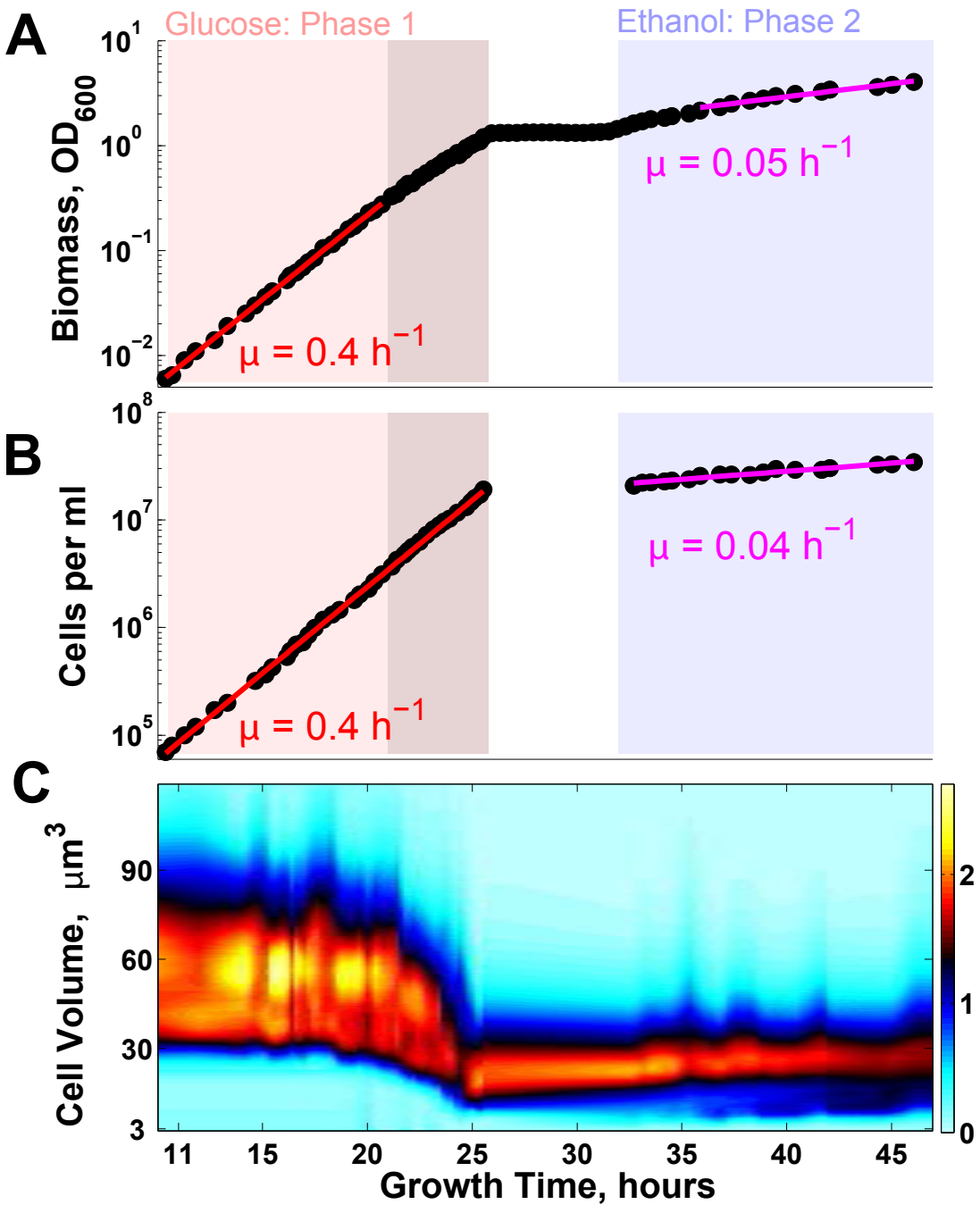
A
Glucose: Phase 1
Ethanol: Phase 2
Biomass, OD600
μ = 0.4 h−1
μ = 0.05 h−1
B
Cells per ml
μ = 0.4 h−1
μ = 0.04 h−1
C
Cell Volume, μm3
Growth Time, hours

Figure S3

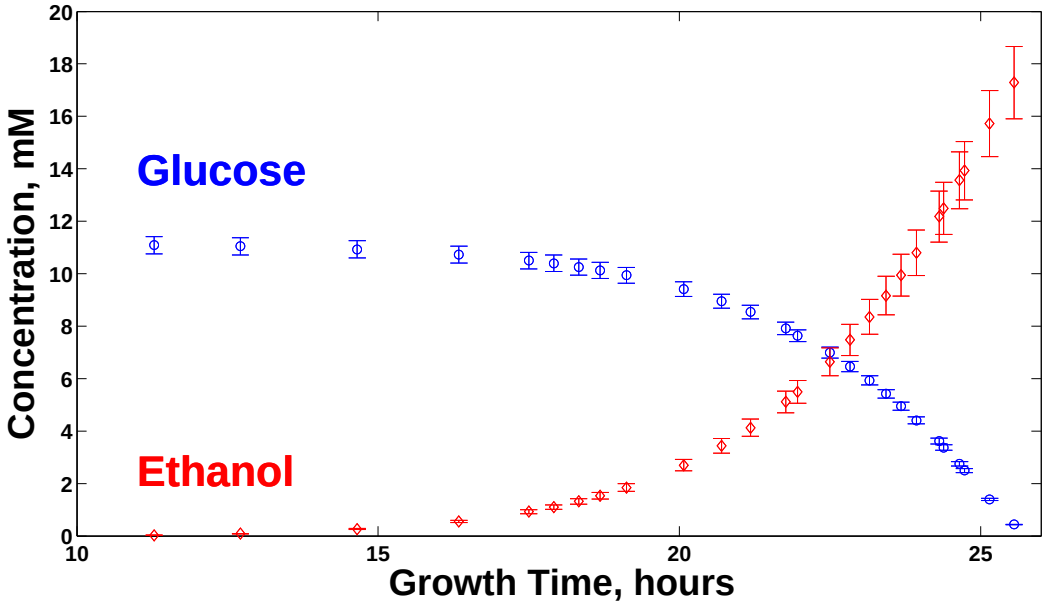
Concentration, mM
Growth Time, hours
Glucose
Ethanol
0
2
4
6
8
10
12
14
16
18
20
10
15
20
25

Figure S4

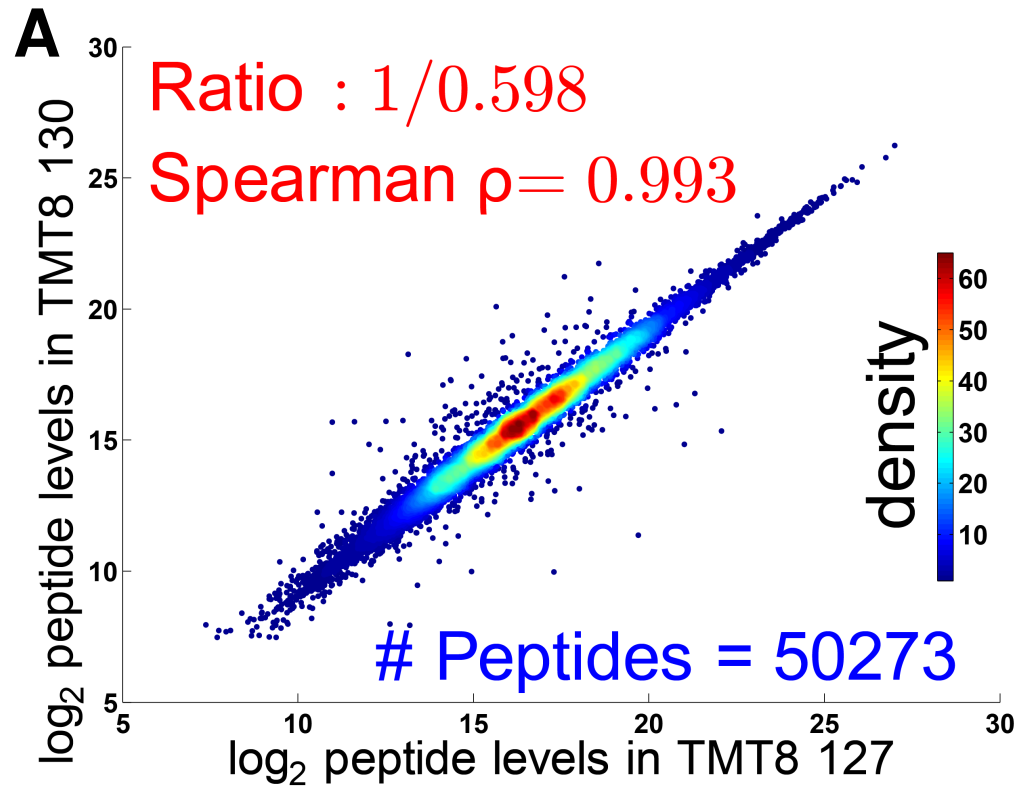
A
Ratio : 1/0.598
Spearman ρ= 0.993
Peptides = 50273
density
60
50
40
30
20
10
log2 peptide levels in TMT8 130
log2 peptide levels in TMT8 127
5
10
15
20
25
30

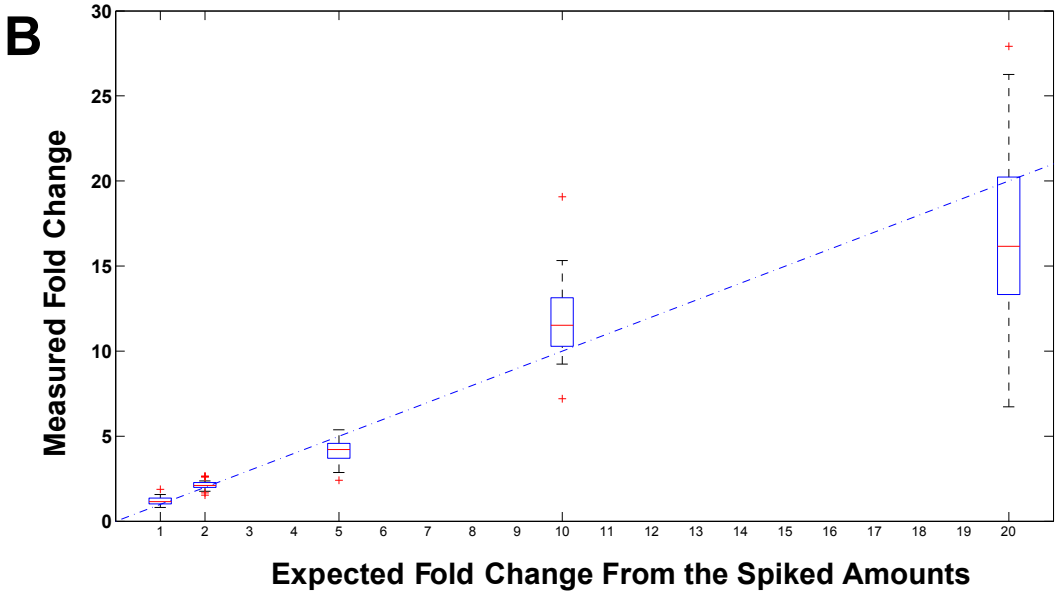
B
Measured Fold Change
Expected Fold Change From the Spiked Amounts
0
5
10
15
20
25
30
1
2
3
4
5
6
7
8
9
10
11
12
13
14
15
16
17
18
19
20

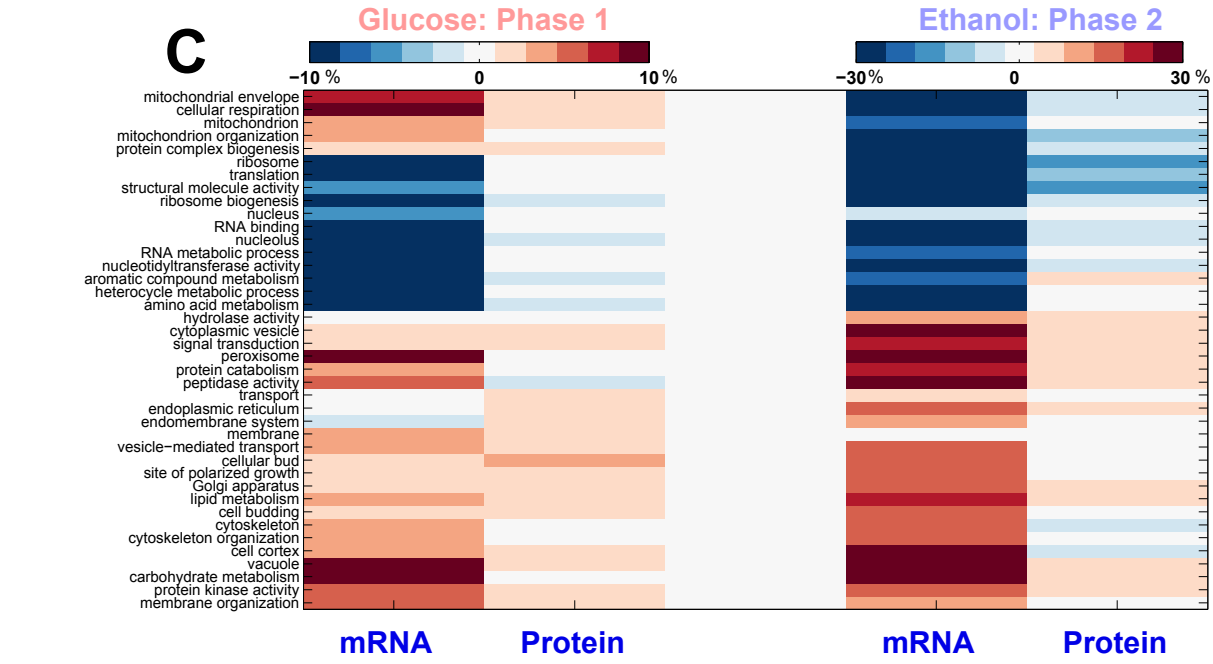
C
Glucose: Phase 1
Ethanol: Phase 2
−10 %
0
10 %
−30 %
0
30 %
mitochondrial envelope
cellular respiration
mitochondrion
mitochondrion organization
protein complex biogenesis
ribosome
translation
structural molecule activity
ribosome biogenesis
nucleus
RNA binding
nucleolus
RNA metabolic process
nucleotidyltransferase activity
aromatic compound metabolism
heterocycle metabolic process
amino acid metabolism
hydrolase activity
cytoplasmic vesicle
signal transduction
peroxisome
protein catabolism
peptidase activity
transport
endoplasmic reticulum
endomembrane system
membrane
vesicle−mediated transport
cellular bud
site of polarized growth
Golgi apparatus
lipid metabolism
cell budding
cytoskeleton
cytoskeleton organization
cell cortex
vacuole
carbohydrate metabolism
protein kinase activity
membrane organization
mRNA
Protein
mRNA
Protein

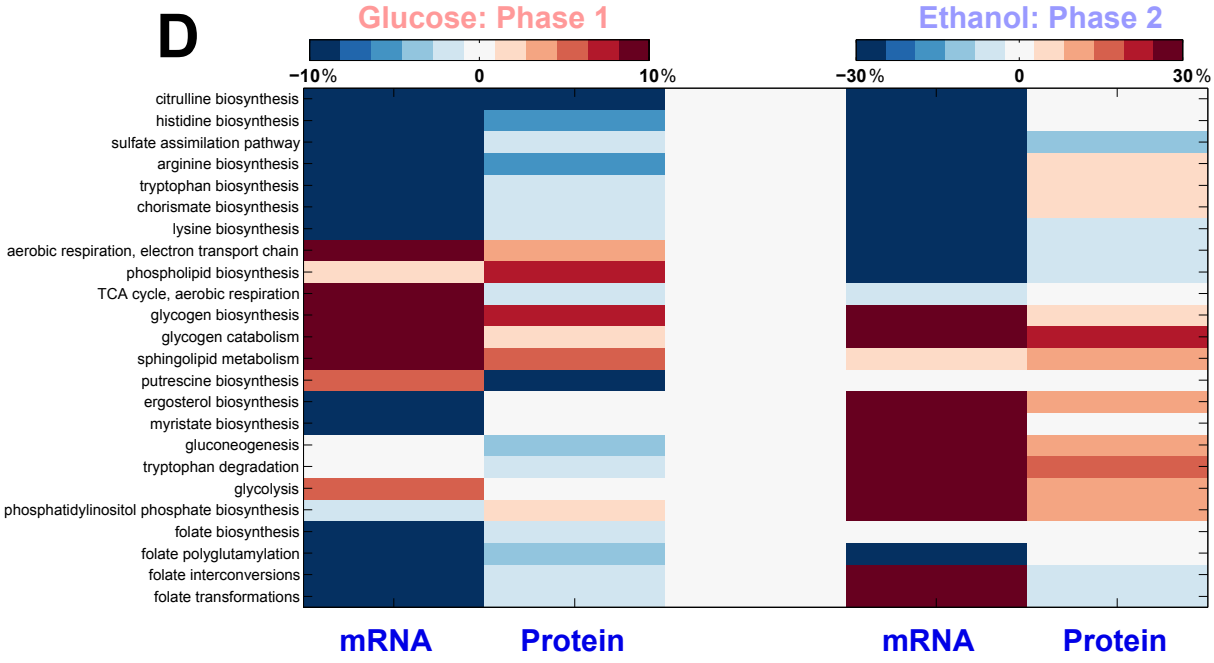
D
Glucose: Phase 1
Ethanol: Phase 2
−10 %
0
10 %
−30 %
0
30 %
citrulline biosynthesis
histidine biosynthesis
sulfate assimilation pathway
arginine biosynthesis
tryptophan biosynthesis
chorismate biosynthesis
lysine biosynthesis
aerobic respiration, electron transport chain
phospholipid biosynthesis
TCA cycle, aerobic respiration
glycogen biosynthesis
glycogen catabolism
sphingolipid metabolism
putrescine biosynthesis
ergosterol biosynthesis
myristate biosynthesis
gluconeogenesis
tryptophan degradation
glycolysis
phosphatidylinositol phosphate biosynthesis
folate biosynthesis
folate polyglutamylation
folate interconversions
folate transformations
mRNA
Protein
mRNA
Protein

Figure S5

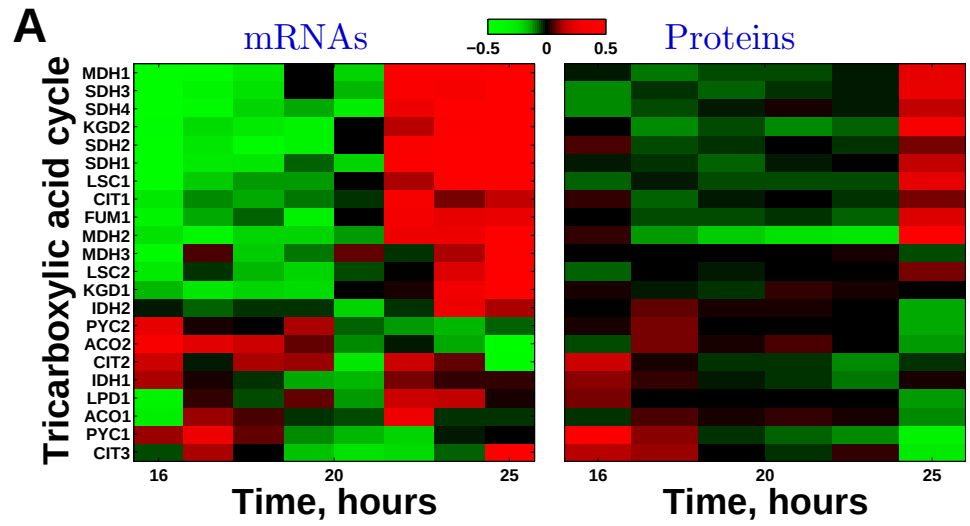
A
mRNAs
−0.5
0
0.5
Proteins
Tricarboxylic acid cycle
MDH1
SDH3
SDH4
KGD2
SDH2
SDH1
LSC1
CIT1
FUM1
MDH2
MDH3
LSC2
KGD1
IDH2
PYC2
ACO2
CIT2
IDH1
LPD1
ACO1
PYC1
CIT3
16
20
25
Time, hours
16
20
25
Time, hours

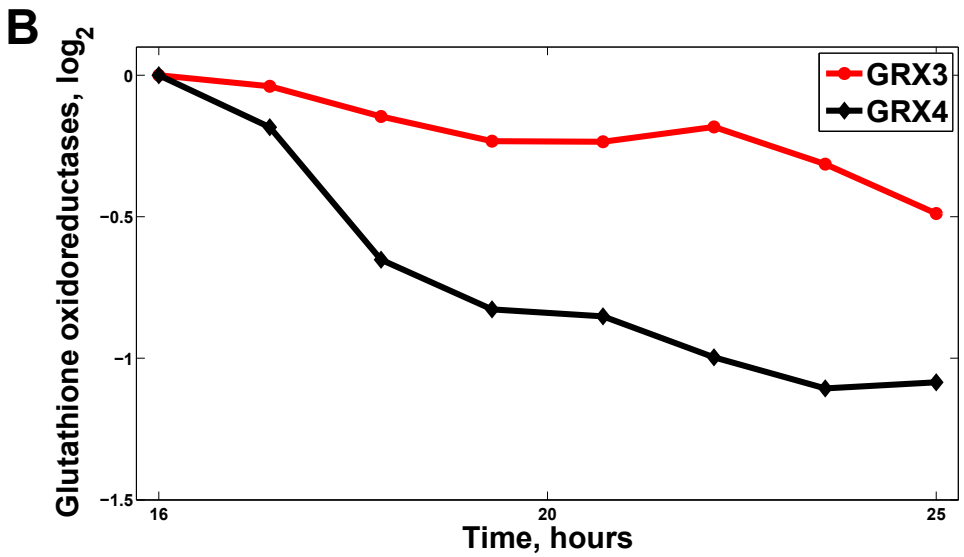
B
Glutathione oxidoreductases, log2
0
−0.5
−1
−1.5
GRX3
GRX4
16
20
25
Time, hours

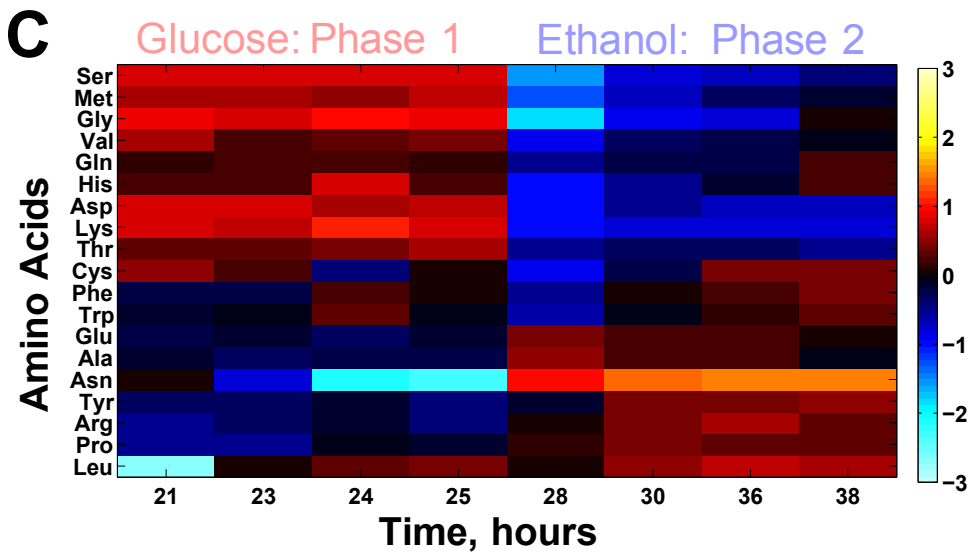
C
Glucose: Phase 1
Ethanol: Phase 2
Amino Acids
Ser
Met
Gly
Val
Gln
His
Asp
Lys
Thr
Cys
Phe
Trp
Glu
Ala
Asn
Tyr
Arg
Pro
Leu
21
23
24
25
28
30
36
38
Time, hours
3
2
1
0
−1
−2
−3

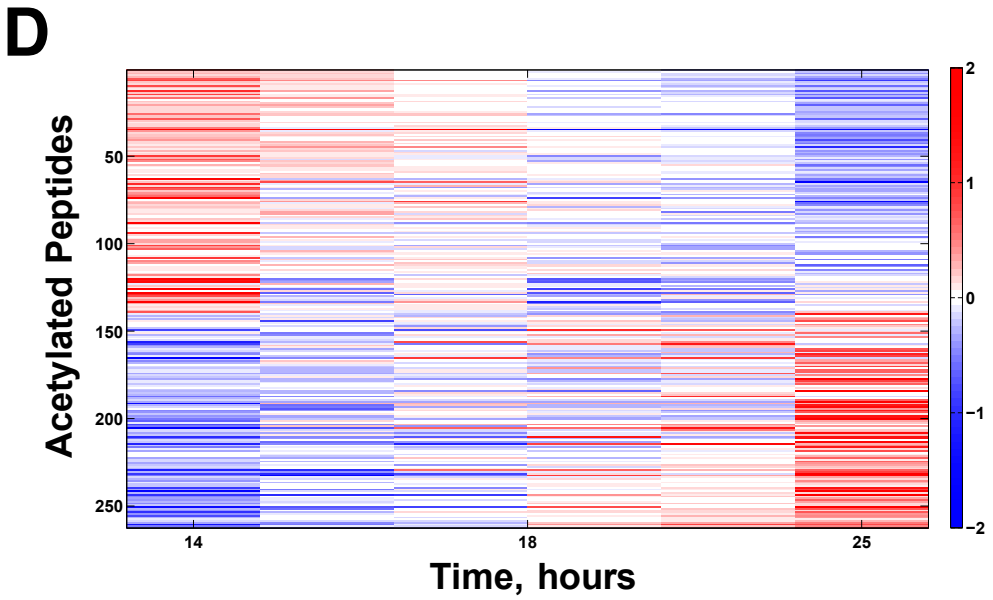
D
Acetylated Peptides
50
100
150
200
250
14
18
25
Time, hours
2
1
0
−1
−2

Table S1. Transcription factors (TF) regulating the transcriptional response during the first phase of exponential growth at a constant rate

Gene Set[a]	TF Name	# TF Target Genes[b]	# Overlapping Genes[c]	p value[d]
Repressed Genes (1356)	Gcn4p	152	74	$< 10^{-20}$
	Fhl1p	143	63	$< 10^{-9}$
	Bas1p	34	21	$< 10^{-7}$
	Met4p	11	8	$< 10^{-4}$
	Met32p	21	12	$< 10^{-4}$
	Aab1p	241	74	$< 10^{-3}$
	Gln3p	67	26	$< 10^{-3}$
	Sfp1p	32	14	$< 10^{-3}$
	Arg81p	15	8	$< 10^{-3}$
	Leu3p	21	10	$< 10^{-3}$
	Rap1p	105	37	$< 10^{-3}$
Induced Genes (1163)	Fkh2p	100	37	$< 10^{-5}$
	Msn4p	73	27	$< 10^{-4}$
	Msn2p	89	30	$< 10^{-3}$
	Aft2p	89	28	$< 10^{-3}$
	Aft1p	66	21	$< 10^{-3}$

[a]Sets of genes (number in the set shown in parentheses) whose mRNA levels either increase or decrease during the first phase of exponential growth at FDR $< 1\%$
[b]Number of genes regulated by the TF according to MacIsaac et al. (2006).
[c]Number of TF target genes found in the gene set.
[d]Probability for observing this or larger number of overlapping genes by chance.